THE DETERMINATION OF EFFECTIVE THICKNESSES
FROM TRANSMISSION MEASUREMENTS
WITH GAMMA RAYS

by

Pierre Goulet

B.Sc.A., Ecole Polytechnique, 1973

A THESIS SUBMITTED IN PARTIAL FULFILMENT OF

THE REQUIREMENTS FOR THE DEGREE OF

MASTER OF APPLIED SCIENCE

in the Department

of

Physics

We accept this thesis as conforming to the
required standard

THE UNIVERSITY OF BRITISH COLUMBIA

April, 1975

In presenting this thesis in partial fulfilment of the requirements for an advanced degree at the University of British Columbia, I agree that the Library shall make it freely available for reference and study. I further agree that permission for extensive copying of this thesis for scholarly purposes may be granted by the Head of my Department or by his representatives. It is understood that copying or publication of this thesis for financial gain shall not be allowed without my written permission.

Department of ___Physics_____

The University of British Columbia
Vancouver 8, Canada

Date ___April 1/1975._____

_6

ABSTRACT

The usual starting point for clinical dosimetry is the dose distribution due to a radiation beam in a homogeneous medium like water. The modification of the standard distribution for the case of an inhomogeneous medium (patient) requires detailed information about internal structures. For heavy charged particle beams and for photon beams of high enough energy, the single parameter which most nearly determines the penetration of the radiation is the electron density (electrons/cm^3). The integrated electron density along a path (electrons/cm^2) is uniquely related to the narrow-beam γ-ray transmission along that path. Hence, a measurement of γ-ray transmission should provide useful information.

This work describes a new technique for performing these measurements. We have used a ^{60}Co therapy source with a rectangular field long enough in one direction to span the width of a human cross section and narrow in the other direction to minimize the effects of scattered radiation. Rather than collimate our detectors, we have devised a simple mathematical procedure to calculate the scatter contribution at each point of interest along the width of the radiation field. Narrow-beam transmission values can then be evaluated from the original measurements by simple substraction of this scatter contribution.

An ionization chamber, because of its energy independence and accuracy, was used to acquire the basic transmission data. X-ray film and silicon diodes, because of their superior resolution and response speed, were selected for the measurements performed with an inhomogeneous phantom. The energy dependence of the latter dosimeters has not been a drawback when used in the experimental conditions described here.

The method thus permits that rapid transmission measurements be performed along various paths of a transverse cross section. When tested with an inhomogeneous phantom, the accuracy obtained compares favourably with published values using collimated detectors.

Information obtained by this method is directly applicable to the dosimetry of treatments performed with photon beams of energy greater than 0.6 MeV and heavy charged particle beams like protons and π^- mesons.

TABLE OF CONTENTS

TABLE OF CONTENTS (CONTINUED)

LIST OF TABLES

LIST OF TABLES (CONTINUED)

LIST OF FIGURES

LIST OF FIGURES (CONTINUED)

1. INTRODUCTION

Routine radiotherapy treatment planning involves the calculation of the dose delivered to a tumour and the surrounding tissues. These dosimetry estimates, because of the similitude between most tissues and water, are usually made on the basis of measurements performed within a water phantom which is approximately a cube of 30 cm a side. Corrections are then applied to take into account the exact contour of the patient and the presence of tissue inhomogeneities, primarily lungs and bones.

In order to calculate the effect of these inhomogeneities on the absorbed dose distribution, various information is required. For each patient, one would like an anatomical cross section where the boundaries of regions with differing attenuation properties could be localized. In general, the chemical composition and density of the tissues are of interest.

Technological constraints, in the past, have made the acquisition of accurate cross-section data difficult. Recently, however, versions of transaxial tomography units, featuring horizontal couches, have been employed clinically for this purpose [Marinello et al. (1), Houdek et al. (2)]. Moreover, a complete cross-section atlas, produced with such an instrument, has recently been published by Takahashi (3). The accuracy attainable has been shown (1,2) to be of the order of 0.2 cm for the external contour of a test phantom. If this accuracy is maintained for internal structures, the method appears capable of providing a suitable cross-section map of a patient. There are other methods, such as ultrasonography, which could be used to give similar and additional information.

Most conventional radiation therapy treatments make use of photons with energies greater than 0.6 MeV. Over this range, for materials of low atomic number such as all biological materials, Compton scattering is the predominant interaction process. Therefore, the linear attenuation coefficient, μ, is proportional to ρ_e, the electron density, where

$$\rho_e = \rho(Z/A)N_a \quad (\text{electrons/cm}^3) \tag{1}$$

and ρ = density of the material.
   Z = atomic number of the material.
   A = mass number of the material.
   N_a = Avogadro's constant.

Since the linear stopping power of heavy charged particles is also, to a good approximation, proportional to ρ_e, this quantity should also be useful in the dosimetry of beams of pions and protons.

Calculations of μ/ρ, assuming incident photons of 1.25 Mev and using mass attenuation coefficients due to Hubbell (4) for the various elements specified in the material's chemical composition, are presented in tables I and II. As shown, μ/ρ is approximately constant for various tissues and for the different compositions of a particular one. The attenuation process of both particle and photon beams is thus strongly dependent of the density of the irradiated tissues. Table III gives a range of densities for normal biological materials.

While the large variations indicated by these figures would seem to warrant the determination of tissue electron densities in individual cases, they primarily point out the necessity of defining acceptable accuracy limits of dosimetry calculations. The American Association of Physicists in Medicine (AAPM) has defined "the criteria for acceptable dosimetry" as "an agreement to ± 3% on exposure or absorbed dose measurement and agreement to ± 5% on fulfillment of tumor dose prescription" (13).

TABLE I

MASS ATTENUATION COEFFICIENTS OF 1.25 MeV
PHOTONS IN VARIOUS HUMAN TISSUES ASSUMING
THE CHEMICAL COMPOSITIONS OF KIM (5)

Tissue	μ/ρ (cm^2/g)
Bone (compact)	.0597
Bone (spongy)	.0611
Brain	.0614
Lung	.0627
Muscle (lean somatic)	.0625

TABLE II

MASS ATTENUATION COEFFICIENTS OF 1.25 MeV
PHOTONS IN COMPACT BONE

μ/ρ (cm^2/g)	Chemical composition reference
.0585	Woodard (6)
.0597	Kim (5)
.0603	ICRU (7)
.0608	Tipton and Cook (8)

TABLE III

DENSITY OF VARIOUS NORMAL TISSUES

Tissue	Density, ρ (g/cm^3)	Reference*
Brain	1.07	Allen (9), Kim (5)
Bone (ribs)	1.09-1.25	Debois & de Roo (10)
Bone (femur)	1.47-2.10	Id.
Bone (vertebrae, mandible)	1.14-1.65	Id.
Heart	1.05	Allen (9), Kim (5)
Kidney	1.04	Id.
Liver	1.05	Id.
Lung	0.25-0.4	ICRU (11)
Muscle (lean)	1.07	Allen (9), Kim (5)
Muscle (striated)	1.00	Spiers (12)
Spleen	1.05	Allen (9), Kim (5)

* The data of Allen et al. (9) give the density of fat-free tissues. These densities were corrected to that of average tissues using the biochemical compositions quoted by Kim (5).

For a ^{60}Co beam, this uncertainty of ± 5% corresponds to an equivalent thickness change of approximately ± 1.0 cm. The equivalent thickness of a material is the thickness of water necessary to produce the same attenuation. However, because of unavoidable uncertainties such as patient movement, for example, a more realistic guideline for the uncertainties permissible was felt to be an equivalent thickness of ± 0.5 cm.

Various workers have proposed γ-ray transmission techniques to determine equivalent thicknesses of human tissues. The basic method is that of Holt and Laughlin (14) where a small collimated ^{60}Co source and collimated scintillation detector are moved laterally across the patient by 2 cm increments. Pulse-height discrimination is employed to reject the detected scatter. The transmission measurements are thus performed in narrow-beam geometry. While basically excellent, the method does necessitate a period of approximately 30 minutes to complete a full cross-sectional survey. This was felt to be not acceptable clinically.

The other published methods of interest have made use of ^{60}Co therapy sources. They were developed for the dosimetry of treatment procedures where a knowledge of the equivalent thicknesses present between two opposing fields is sufficient (i.e., complete rotation fields, opposing pair of fixed fields). The measurements were performed, in all cases, along the central axis of standard field sizes, often corresponding to those used during the actual treatment. Various techniques have been proposed to eliminate or take into account the scatter reaching the detector. Pfalzner (15) used an ion chamber positioned at 70 cm behind the patient to minimize this scatter. Fedoruk and Johns (16) proposed a heavily collimated ionization chamber to be used at a closer distance to the patient. Another method due to Woodley et al. (17) consisted in placing

a thin-window ion chamber directly behind the patient. From the exit doses recorded, equivalent thicknesses could then be inferred from calibration curves determined for specific field sizes. The methods (15,16) involve the relative rotation of both source and detector about the patient and could be used to provide a complete cross-sectional survey. The disadvantage of this approach, however, is that the information obtained is too heavily weighted toward the centre while neglecting the outer edges of the body cross section.

Because of this, we felt an investigation of a different method of obtaining clinically useful transmission data using a standard therapy source was warranted. It was decided to use a rectangular radiation beam with its longitudinal dimension large enough to span the transverse cross section to be measured, the other field dimension being narrow to minimize scattered radiation. Transmission determinations along a large number of paths could then be performed rapidly if film or a light-weight scanning detector is used. The major difficulty, however, is the elimination of the produced scatter. It was felt that collimating our detector would be impractical. Instead, we chose to devise a simple mathematical procedure to determine the scatter contribution at each measurement point. It is possible by this technique to obtain narrow-beam transmission data from the original measurements by mathematically subtracting the scatter and thus to determine the equivalent thickness along each γ-ray path of interest. Measurements of an inhomogeneous phantom were performed to test the validity of the method and, as will be shown, the agreement between the equivalent thicknesses calculated from the transmission data and those calculated from the phantom's geometry and composition was better than $\pm$ 0.5 cm.

2. BASIC TRANSMISSION MEASUREMENTS

2.1 Introduction

The amount of scatter reaching the detector in a transmission measurement depends on a number of factors. Consider the geometry used for such a measurement shown in figure 1. Various parameters will influence the amount of scatter measured. In particular,

(a) An increase of the absorber-to-detector distance, B, will decrease the scatter reaching the detector.

(b) An increase of the field size, S, will increase the scatter. Note that field dimensions throughout this paper are quoted as measured at a distance A from the source.

It was found convenient to choose A equal to 120 ± 0.5 cm. We then investigated the effect of independently varying the distance B and the field area on the relative transmitted dose, T. This quantity is the quotient of the dose measured with an absorber present in the beam path by that measured with no absorber. Mathematically, the relative dose transmitted by an absorber of thickness, t, can be expressed, for a specific absorbing material, as

$$T \equiv T(P,B,S,t) \qquad\qquad (2)$$

where P describes the position of the measurement point, usually the distance off the central axis of the field.

Table IV lists the various experimental conditions investigated. The radiation source used was housed in a commercial therapy unit (Atomic Energy of Canada Ltd., Eldorado Model 8) equipped with a sloping sided collimator. Most measurements were performed with a Baldwin-Farmer 0.6 cm^3
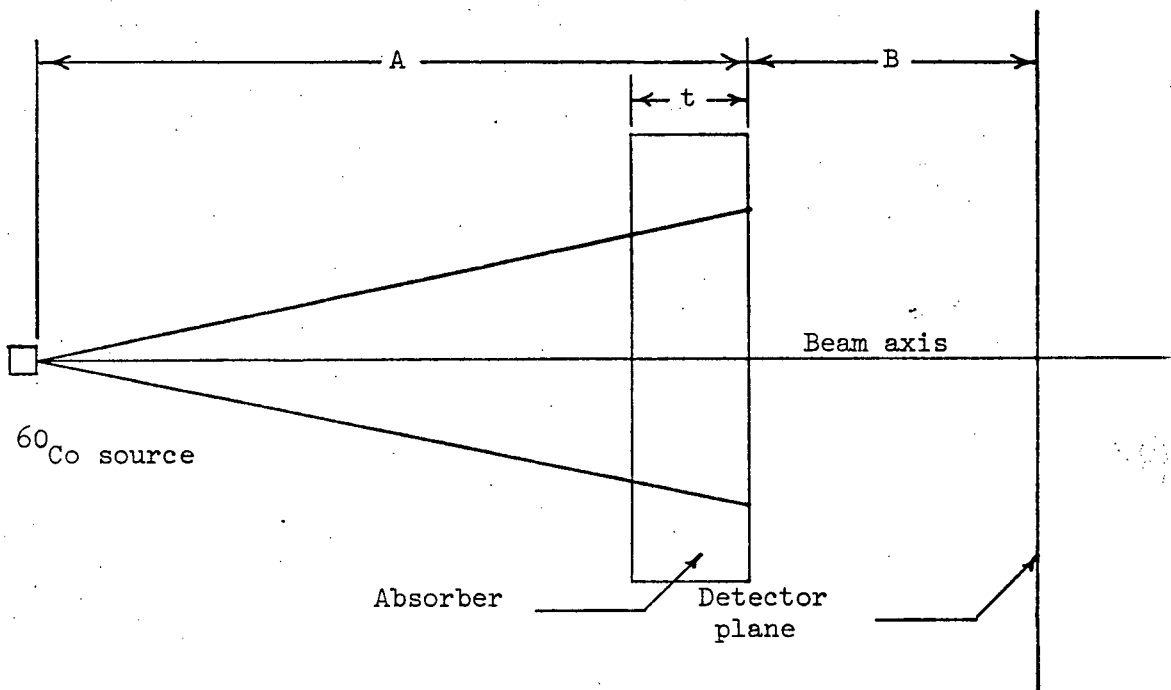
FIGURE 1 EXPERIMENTAL LAYOUT USED TO PERFORM TRANSMISSION MEASUREMENTS

TABLE IV

SYNOPSIS OF MEASUREMENTS PERFORMED

Field shape	Material	Absorber thickness (cm)	A (cm)	B (cm)	Section
Square	Water	18.106	120	0, 15, 30 45, 60	2.2.1
Square	Al	2.592	120	35, 55, 75	2.2.2
Square	Pb	2.519	120	35, 55	2.2.2
Rectangular	Water	9.436, 13.443 18.106, 24.136	120	30	2.3.1
Rectangular (off-axis)	Water	18.106, 24.136	120	30	2.3.2

ionization chamber polarized by 300 volts. The ionization current was integrated by an electrometer (Keithley, Model 610C) for one minute periods. A voltage proportional to this charge was read with a digital voltmeter. Both leakage and environmental conditions were monitored. Their effects were less than the statistical variation of the measurements ($\pm$ 0.15% on the average) and were not corrected for.

2.2 Transmission Measurements with Square Fields

2.2.1 Measurements using a large water absorber

A large water phantom of uniform thickness was first used to measure T along the central axis for various beam areas. Table V shows the data obtained with a 18.106 cm thick absorber. Additional measurements with a 24.136 cm water thickness showed a similar trend.

The variation of T with area, for a fixed B, is fitted to better than the experimental accuracy ($\pm$ 0.3% on the average) by a quadratic

TABLE V

MEASURED RELATIVE TRANSMISSION USING
SQUARE BEAMS FOR A THICK WATER ABSORBER

Field area at 120 cm from the source (cm^2)	$T(0,B,S,18.106)$			
	B=15 cm	B=30 cm	B=45 cm	B=60 cm
441	.4029	.3634	.3451	.3339
324	.3875	.3520	.3362	.3275
225	.3710	.3402	.3277	.3221
144	.3529	.3297	.3199	.3158
81	.3350	.3193	.3132	.3114
36	.3205	.3116	.3090	.3076
Zero extrapolation	.3093	.3054	.3050	.3048

equation using a least-squares method. The zero-area extrapolation calculated from such a fit is indicated in table V. Except for the value obtained with B equal to 15 cm, these extrapolated values lie within 0.3% of each other. From these latter figures the zero-area linear attenuation coefficient, μ_0, was estimated to be .0656 ± .0002 cm^{-1}. Further discussion of this result will be presented later.

Figure 2 illustrates the variation of T with distance B for field sizes of 36 and 225 cm^2 respectively. The exit doses (B = 0) were measured with a thin-window ionization chamber in direct contact with the absorber. The centre of the flat cylindrical cavity lies 0.1 cm below the thin mylar window. The procedure and readout circuit previously described were again used. A buildup cap of 0.5 cm of water-equivalent material was employed in the absence of the absorber. The ion chamber was polarized by 45 volts and a correction was applied for the small leakage current present.
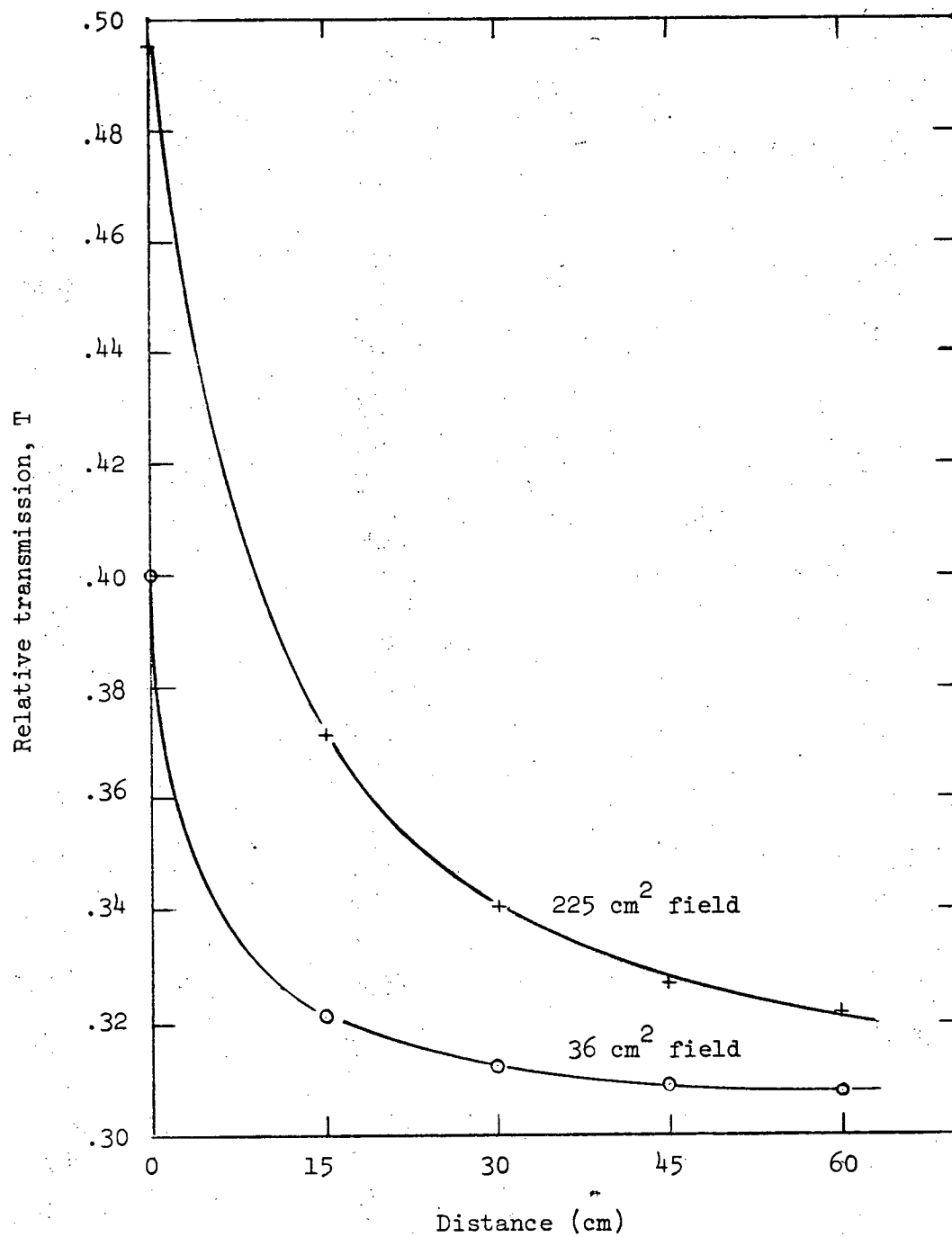
FIGURE 2   TRANSMISSION MEASUREMENTS SHOWING THE EFFECT OF
MODIFYING THE ABSORBER-TO-DETECTOR DISTANCE

We attempted to compare published results to our experimental data. Results similar to those of figure 2 were presented by Fedoruk and Johns (16) for distances extending from 5 to 20 cm. Interpretation of their data is made difficult, however, by the fact that the experimental layout is not specified. Moreover, they do not state where the quoted field dimensions were measured. Pfalzner (15) commented that at 70 cm from the absorber "the scatter contribution has been found experimentally to be negligible". Since no details of the radiation beam dimensions were provided, one is led to assume that the statement applies to all field sizes. The criterion used to define acceptability was not stated.

2.2.2 Measurements using thick Al and Pb absorbers

It is known that the spectrum emitted from a ^{60}Co teletherapy source contains low energy components. This is due to scatter from the source itself, the source housing, the collimator and the interposed air column between the source and the detector. Published calculations (18), using Monte Carlo techniques, have been performed to determine the spectrum from a ^{60}Co source. However, because of the complexity and variability of the collimator geometry, the scatter contribution from it was ignored. Since the narrow-beam attenuation coefficients derived from our measurements also exclude collimator scatter, a realistic comparison of the Monte Carlo calculations and the experiments seems possible.

In an effort to further characterise the composition of the photon spectrum, transmission measurements were performed with materials of higher atomic number. Aluminium ($\rho = 2.70$ g/cm^3) and lead ($\rho = 11.34$ g/cm^3) were used and the results appear in table VI. The distance B was larger than 30 cm to facilitate zero-area extrapolation. Least-squares

TABLE VI

MEASURED RELATIVE TRANSMISSION USING SQUARE
BEAMS FOR THICK Al AND Pb ABSORBERS

ALUMINIUM ABSORBER			
Field area at 120 cm from the source (cm^2)	T(0,B,S,2.592)		
	B=35 cm	B=55 cm	B=75 cm
380.3	--	.6904	.6837
324	.7033	--	--
272.3	--	.6851	.6797
225	.6950	--	--
182.3	--	.6792	.6753
144	.6866	--	--
110.3	--	.6755	.6726
81	.6785	.6732	.6710
36	.6733	.6707	.6698
Zero extrapolation	.6685	.6679	.6678

LEAD ABSORBER		
Field area at 120 cm from the source (cm^2)	T(0,B,S,2.519)	
	B=35 cm	B=55 cm
95	.1911	.1855
81	.1899	.1845
72	.1886	.1838
56.3	.1868	.1832
36	.1848	.1820
Zero extrapolation	.1810	.1800

curve fitting techniques were again employed; a quadratic equation was used for the aluminium data while a straight line was found satisfactory for the lead data.

Calculations of μ_0 for water, aluminium and lead were done using a published spectrum [ICRU (18)] based on the model of figure 3. Note that the scatter due to the source housing is ignored. Table VII compares the parameters of this model to those of the actual source. For calculation purposes the following was assumed:

(a) Photons emitted from the front surface of the tungsten sleeve are considered to be absorbed by the collimating system and not reach the detector.

(b) Photons emitted from the front surface of the core are attenuated by a stainless steel (type #316L) plate of 0.11 cm thickness.

The calculated values of μ_0 are shown in table VIII with the corresponding experimental results. The experimental value in the Table for water was obtained from rectangular beam data and will be discussed later. Attenuation coefficients from Hubbell's compilation (4) were used in all cases except for lead where the work of Storm and Israel (19) was also used. The variation in the calculated μ_0 for the case of lead lies within the accuracy limits specified by the latter authors:

(a) Accuracy of 3% for Compton scatter coefficients.

(b) Accuracy of 3% for photoelectric coefficients at photon energies $h\nu$ such that $.006 < h\nu < .200$ MeV.

(c) Accuracy of 10% for photoelectric coefficients at energies $h\nu > .200$ MeV.

Agreement between calculated and measured values is good. Since

Plane view of cylindrical source
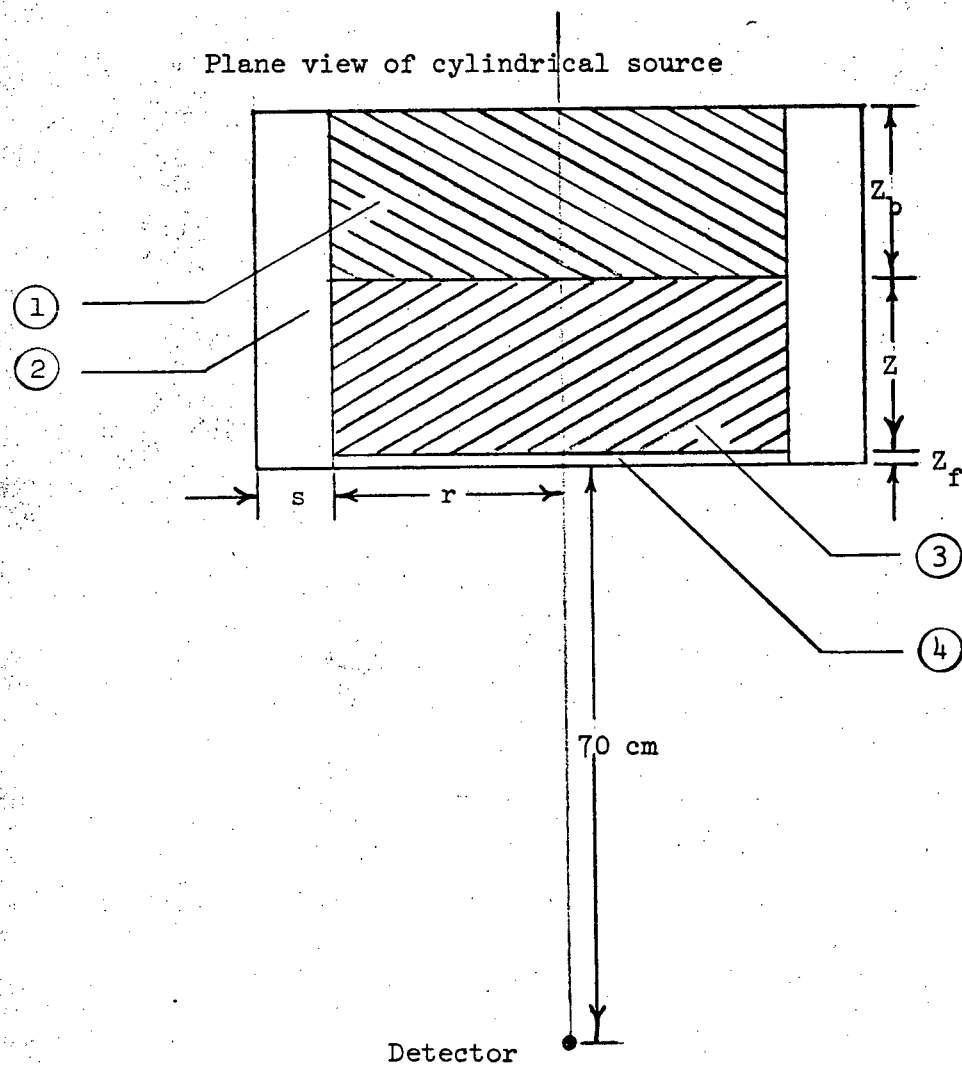
① Steel back plate

② Cylindrical tungsten sleeve

③ Radioactive core

④ Steel front plate

FIGURE 3   MODEL USED TO REPRESENT THE ^{60}Co SOURCE AND ITS

SURROUNDING SLEEVE

[Adapted from reference (18)]

TABLE VII

DETAILS OF THE APPROXIMATE AND ACTUAL SOURCE

Parameter*	Model	Actual source
r (cm)	1.0	1.0
s (cm)	0.75	0.86**
Z (cm)	1.3	2.5
Z_b (cm)	2.2	1.1
Z_f (cm)	0.0	0.11
Packing density (g/cm^3)	5.88	5.61

* See figure 3.
** Does not include the source's stainless steel
   wall of 0.14 cm thickness.

TABLE VIII

CALCULATED NARROW-BEAM ATTENUATION COEFFICIENTS OF RADIATION
FROM A ^{60}Co THERAPY SOURCE FOR VARIOUS MATERIALS

Material	Measured μ_0 (cm^{-1})	Calculated μ_0 (cm^{-1})	Origin of attenuation coefficient data
H_2O	.0653	.0648	Hubbell (4)
Al	.156	.154	Id.
Pb	.680	.686	Id.
Pb	.680	.669	Storm & Israel (19)

the scatter contributed by the source housing was neglected during the calculation, we would expect slightly larger attenuation coefficients to be observed experimentally. While this is indeed the case, the statistical significance of this trend is difficult to determine. We can only conclude that the actual beam probably possesses a spectrum of similar shape to that of our assumed one.

2.2.3 Calculation of the first scatter contribution

The calculation of the amount of radiation scattered from thick slabs irradiated by finite area beams can only be adequately performed using a Monte Carlo procedure. However, the first scatter contribution may be derived exactly from the Klein-Nishina equations. This was done here for various water thicknesses irradiated by 36 and 225 cm^2 circular fields of 1.25 MeV photons under two specific geometries.

The case where the detector is 30 cm from the absorber was investigated first. Figure 4(a) illustrates the observed results. The full line is drawn through the calculated first scatter points derived from the general method outlined in appendix A. The circles are experimental results and represent the total scatter contribution expressed as the function Δ where

$$\Delta(0,30,S,t) = T(0,30,S,t) - T(0,30,0,t)$$

where $\qquad T(0,30,0,t) = \exp(-\mu_0 t)$ $\qquad\qquad\qquad$ (3)

Similarly, $\Delta_1(0,30,S,t)$ is the calculated increase in relative transmission due to first scatter only.

The general shape observed for Δ_1 can be explained rather simply by the following argument. Neglecting the attenuation of the scattered photons, one would expect the first-order scatter to increase with absorber thickness since the total number of Compton interactions increases with
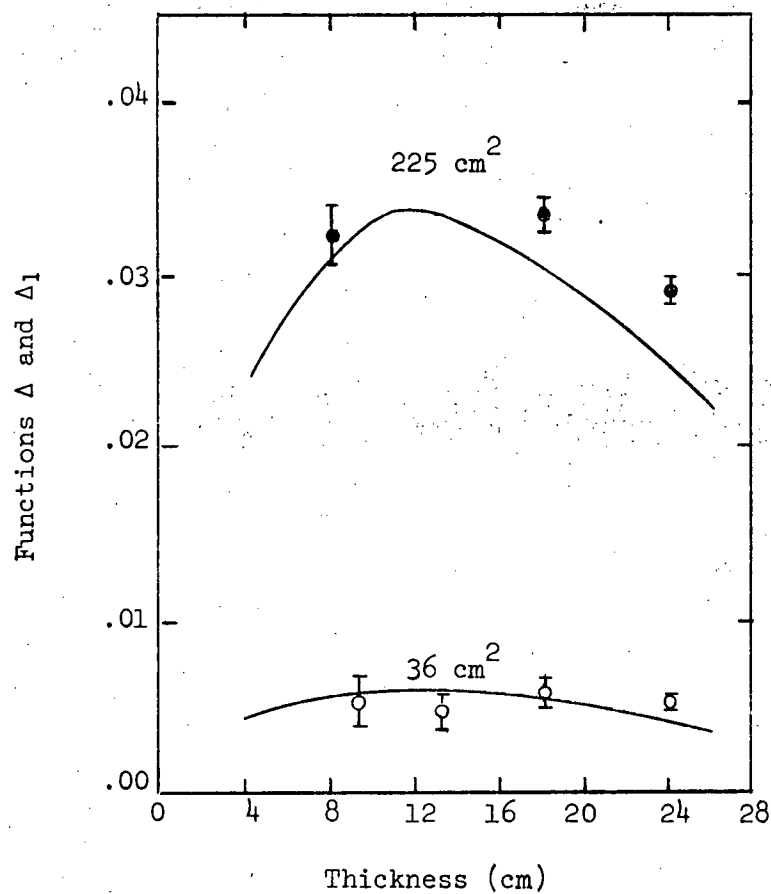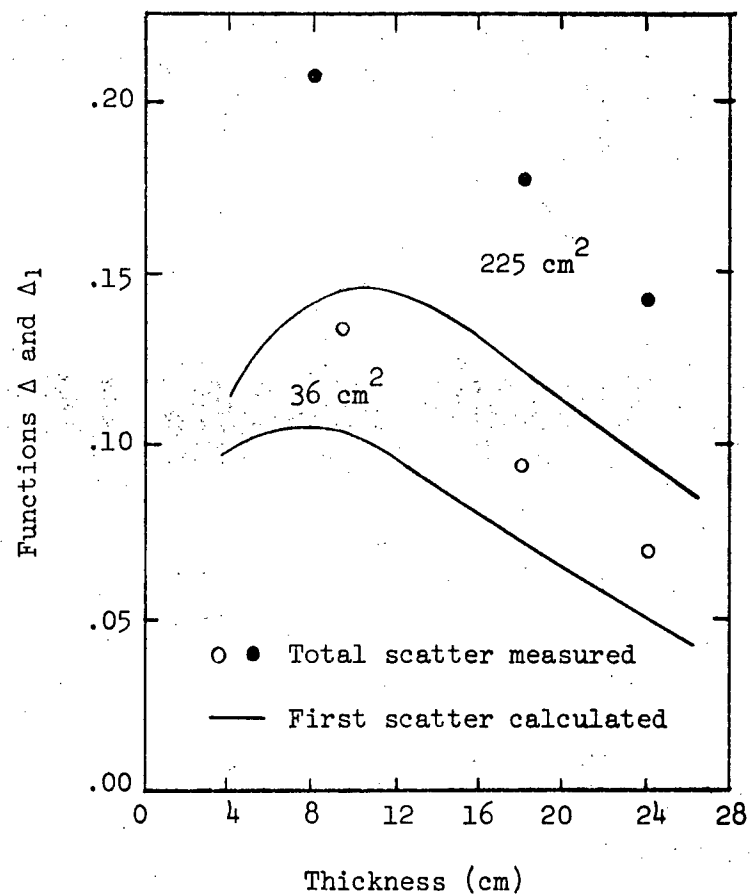
FIGURE 4 COMPARISON OF CALCULATED FIRST SCATTER WITH MEASURED TOTAL SCATTER a) BY A
DOSIMETER PLACED AT 30 cm FROM THE ABSORBER AND b) BY AN EXIT DOSIMETER

the number of electrons present. However, for thick absorbers, the attenuation of the scattered photons cannot be neglected. This effect, because of its exponential form, compensates for the production of once scattered photons for absorbers about 12 cm thick and becomes the dominating process for thicker absorbers.

As the attenuation becomes predominant, the production of multiple scatter also increases. This is demonstrated particularly for the larger area field where the difference, $(\Delta - \Delta_1)$, while being small, increases with the thickness of the water absorber considered.

Since the effect of multiple scatter should be greatest at the exit surface (B = 0), it was decided to compare first scatter calculations to total scatter measurements here. Figure 4(b) presents the results describing the first scatter reaching an exit dosimeter using the method described in appendix B. Also presented are some experimental observations where the total scatter contribution was recorded. The same general shape of the functions Δ and Δ_1 is again observed. The main difference is due to the presence of a large multiple scatter contribution that accounts for a major portion of the total scatter measured.

We have thus characterized the nature of the scatter emitted under two particular conditions. The calculations could be generalized to other similar experimental situations.

2.3 Transmission Measurements Using Rectangular Fields

2.3.1 Central axis measurements

As was previously mentioned, the choice of a long and narrow field would appreciably reduce unwanted scatter while permitting transmission measurements to be performed along the full width of a human

transverse cross section. The Eldorado 8 cobalt unit has a minimum field
dimension of 6 cm at 120 cm from the source. The field length, 2b, can
be varied from 6 to 48 cm. Central axis transmission data was obtained
using water absorbers of 9.436, 13.443, 18.106 and 24.136 cm thicknesses
with field sizes of 6 x 2b cm; 6 < 2b < 48 cm. The detector was positio-
ned at a distance of 30 cm from the absorber. These measurements have
been tabulated in table IX. Each entry is the average of two determina-
tions. The notation has been slightly modified as follows:

$$\Delta(0,30,S,t) \equiv \Delta(0,S,t) \qquad (4)$$

since B remains equal to 30 cm in all subsequent measurements and

$$\Delta(0,S,t) \equiv \Delta(0,b,t) \qquad (5)$$

for a rectangular field of dimension 6 x 2b.

Relative transmitted doses graphically extrapolated to zero
area are presented in table X. From these a value of μ_0 = .0653 ± .0002
cm^{-1} was derived. This value is consistent with that determined previously
from the square field data (μ_0 = .0656 ± .0002 cm^{-1}). Different workers
have reported μ_0 = .066 cm^{-1} [Jones et al. (20), Johns et al. (21)] and
μ_0 = .065 cm^{-1} [Payne et al. (22)] for various therapy units. Our coef-
ficient is in agreement with these.

Figure 5 shows $\Delta(0,b,t)$ expressed as a function of water thick-
ness for various field sizes. We have shown at each point the range of
the two experimentally derived values. The continuous lines indicated
were used in performing the calculations discussed in appendix C. For
thicknesses ranging from 8 to 20 cm, the function was assumed constant
within the experimental limits and numerically equal to the mean of the
data for the 9.436, 13.443 and 18.106 cm thick absorbers. The general
shape of this curve is in agreement with that observed previously using

TABLE IX

RELATIVE TRANSMISSION INCREASE CAUSED BY SCATTERED RADIATION:
CENTRAL AXIS MEASUREMENTS OF WATER SLABS IRRADIATED BY RECTANGULAR BEAMS

Field dimensions, 6 x 2b, at 120 cm from the source (cm)	$\Delta(0,b,t)$			
	t=9.436 cm	13.443 cm	18.106 cm	24.136 cm
6 x 6	.005$_5$	.004$_9$	.005$_9$	.005$_4$
6 x 12	.012$_4$	.011$_4$	.011$_8$	.010$_4$
6 x 18	.017$_0$	.016$_2$	.017$_0$	.014$_3$
6 x 24	.021$_2$	.021$_6$	.021$_4$	.018$_7$
6 x 30	.024$_2$	.024$_8$	.025$_4$	.021$_6$
6 x 36	.027$_4$	.027$_0$	.028$_4$	.024$_6$
6 x 42	.029$_2$	.028$_8$	.029$_6$	.025$_6$

TABLE X

EXTRAPOLATED NARROW-BEAM TRANSMISSION
VALUES FOR WATER

Thickness (cm)	Relative transmission determined by	
	Extrapolation to zero area	Calculation ($\mu_0 = .0653$ cm^{-1})
9.436	.5383	.5400
13.443	.4156	.4157
18.106	.3064	.3066
24.136	.2077	.2068
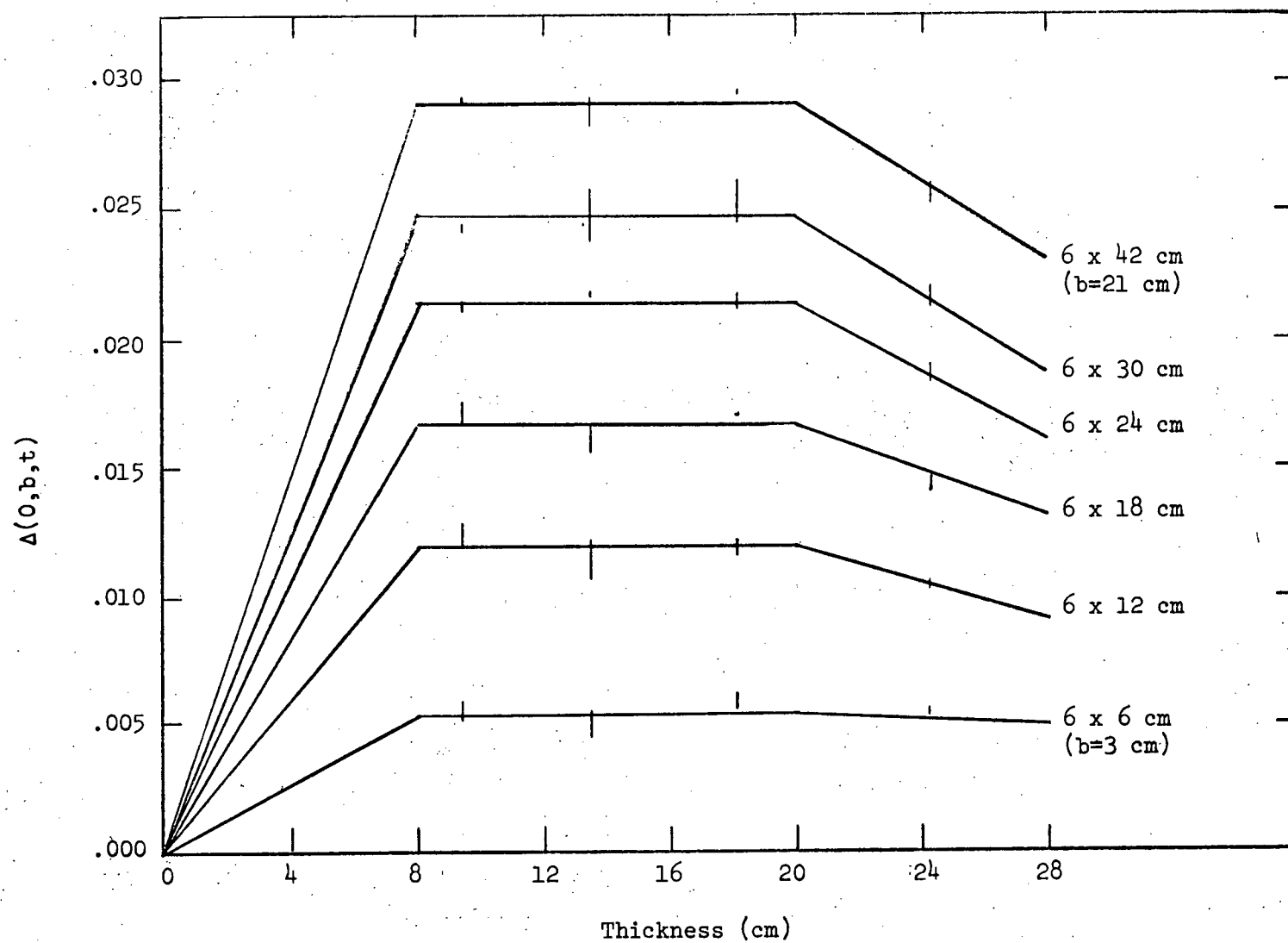
FIGURE 5   VARIATION OF $\Delta(0,b,t)$ FOR VARIOUS ABSORBER THICKNESSES AND FIELD SIZES

square fields of similar areas.

As stated previously, the method of measurement outlined in this paper relies on the development of a mathematical procedure to quantify the scatter reaching the measuring instrument. A convenient procedure is one analogous to the method proposed by Clarkson (23) for depth-dose calculations of irregular fields.

Consider figure 6. The scatter reaching a detector at point 0 can be expressed, assuming the validity of Clarkson's method, as

$$\Delta(0,b,t) = \sum_{i=1}^{n} \frac{1}{n} \Delta(0,S_i,t) \qquad (6)$$

where S_i = area of square field of equivalent radius = πr_i^2.

The validity of equation (6) was verified by calculating $\Delta(0,b,t)$ for a range of field sizes. The comparison with experiment is presented in table XI. The calculation is restricted to a maximum field of 6 x 30 cm because the square field data could not be further extrapolated with

TABLE XI

VALIDITY OF CLARKSON'S METHOD

Field dimensions 6 x 2b, at 120 cm from the source (cm)	$\Delta(0,b,18.106)$	
	Measured	Calculated
6 x 12	$.011_8$	$.012_1$
6 x 18	$.017_0$	$.016_9$
6 x 24	$.021_4$	$.021_4$
6 x 30	$.025_4$	$.024_7$

FIGURE 6   ILLUSTRATION OF CLARKSON' METHOD

FIGURE 7   GEOMETRIC DESCRIPTION OF THE QUANTITIES
USED IN EQUATION (7)

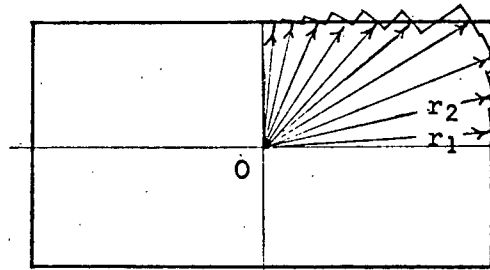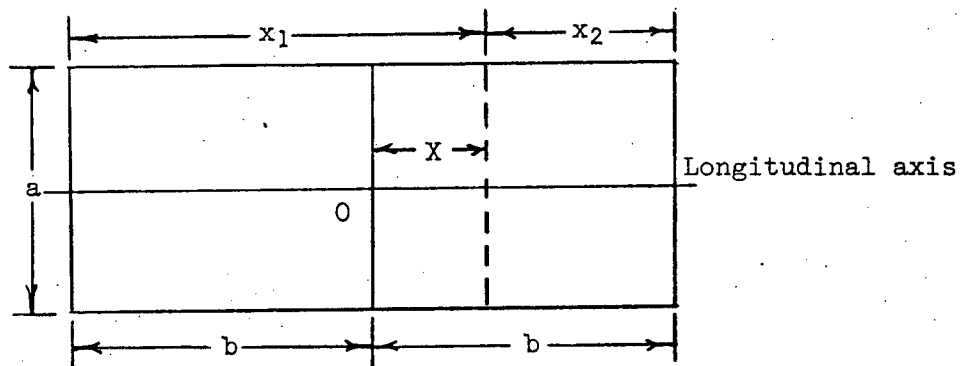confidence. The agreement is good and proves the applicability of a Clarkson-type calculation in this situation.

2.3.2 Off-axis measurements

We now wish to compute the scatter reaching a detector positioned at an arbitrary distance X along the longitudinal axis of a rectangular field. Figure 7 illustrates the relevant geometry.

Then,

$$\Delta(X,b,t) = [\Delta(0,x_1,t) + \Delta(0,x_2,t)]/2 \qquad (7)$$

Assuming $\Delta(X,b,t)$ and $\Delta(0,x_2,t)$ to be known, it is possible to determine

$$\Delta(0,x_1,t) = 2\Delta(X,b,t) - \Delta(0,x_2,t) \qquad (8)$$

It is thus possible, from the above equation, to extend the data of the previous section using the results of off-axis measurements.

These measurements were performed with a field size of 6 x 45 cm and with water thicknesses of 18.106 and 24.136 cm. It was assumed that the results obtained with the former absorber would apply to thicknesses ranging from 8 to 20 cm. The data is presented in figure 8 where the open symbols refer to the original measurements. Each of these was then corrected for the increased attenuation caused by the oblique path travelled by the γ rays through the phantom. These corrected points, shown as full symbols, then represent the relative transmission through an oblique path of 18.106 and 24.136 cm respectively. By using equation (8) and subsequently fitting the obtained results, the values of table XII were determined. Figure 9 collects the data of tables X and XII for thicknesses of 18.106 and 24.136 cm respectively. The dots are the values from the tables while the full line was employed to perform the calculations of appendix C.
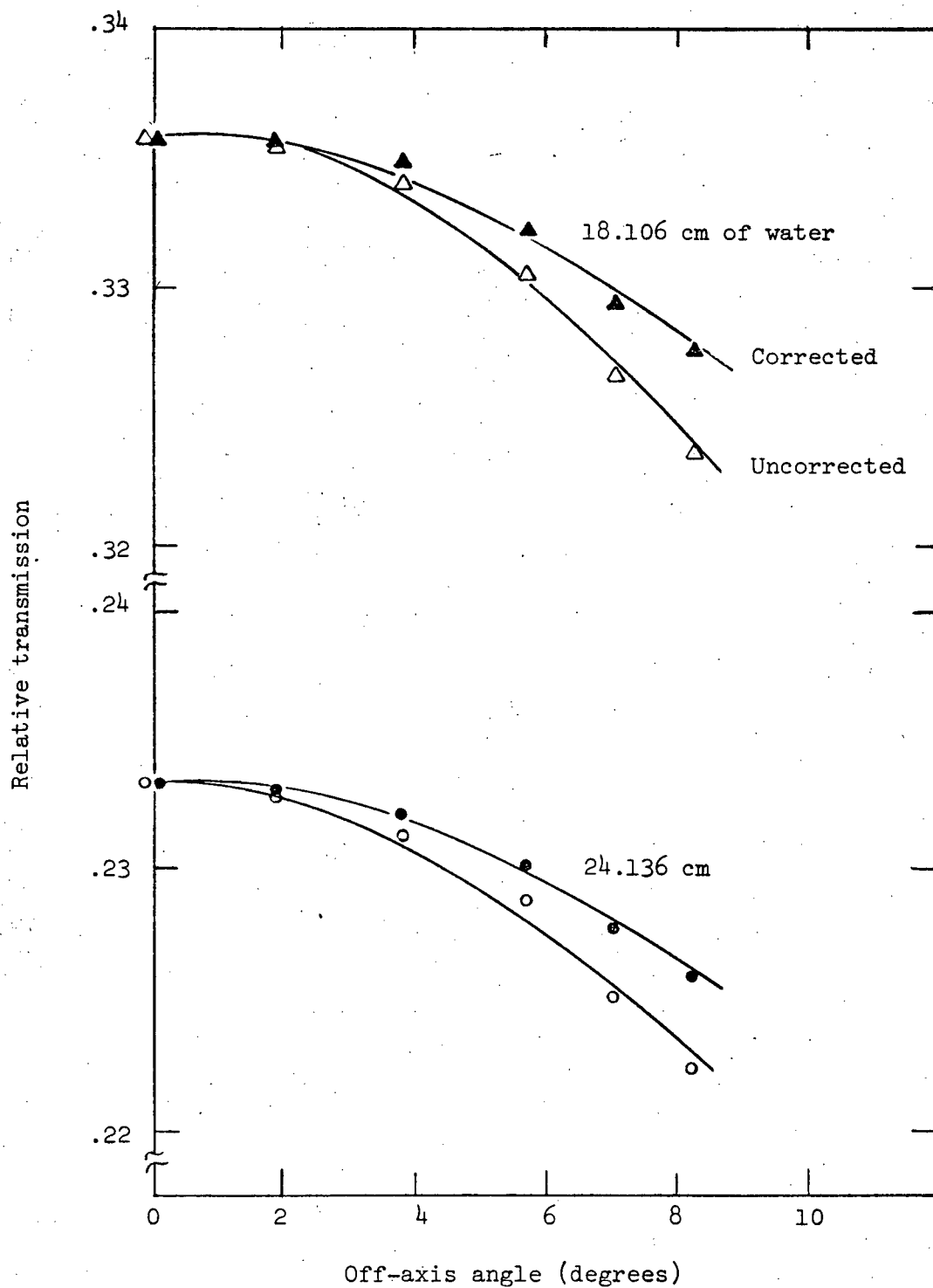
FIGURE 8 RELATIVE TRANSMISSION MEASUREMENTS ALONG THE
LONGITUDINAL AXIS OF A RECTANGULAR FIELD

TABLE XII

RELATIVE TRANSMISSION INCREASE CAUSED BY SCATTERED RADIATION:
CALCULATIONS FROM OFF-AXIS MEASUREMENTS
ALONG THE LONGITUDINAL AXIS OF A RECTANGULAR BEAM

Field dimensions, 6 x 2b, at 120 cm from the source (cm)	$\Delta(0,b,t)$	
	t=18.106 cm	t=24.136 cm
6 x 48	$.030_4$	$.026_8$
6 x 54	$.031_2$	$.027_6$
6 x 60	$.032_1$	$.028_3$
6 x 66	$.032_5$	$.028_8$
6 x 72	$.032_8$	$.029_2$
6 x 78	$.032_9$	$.029_5$
6 x 84	$.033_0$	$.029_7$
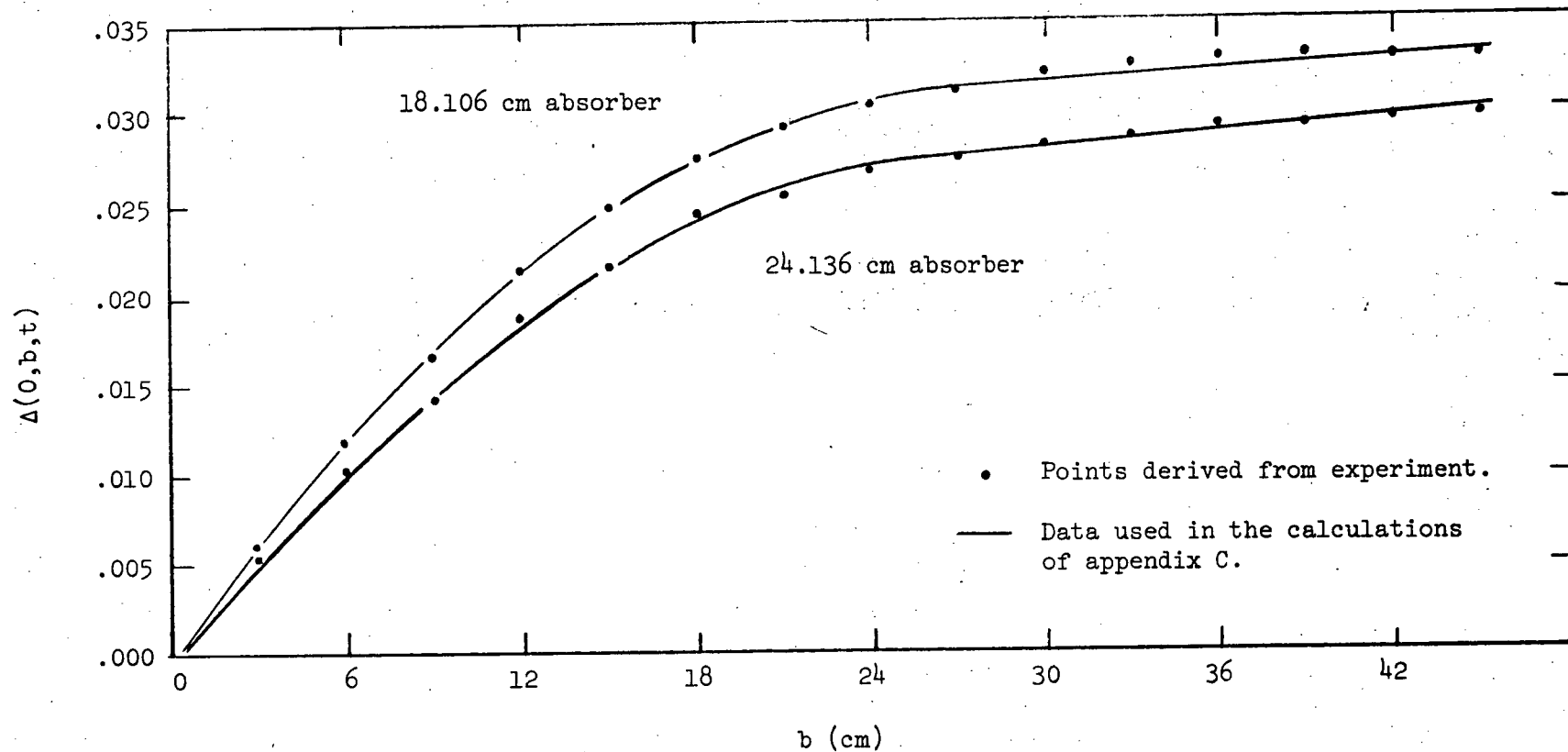
FIGURE 9   THE FUNCTION Δ(0,b,t) AS DETERMINED FROM THE MEASUREMENTS USING RECTANGULAR FIELDS

3. TRANSMISSION MEASUREMENTS WITH AN INHOMOGENEOUS PHANTOM

3.1 Introduction

The basic measurements discussed in the previous chapter have been applied here to the determination of equivalent thicknesses along various paths in an inhomogeneous phantom. Two new detecting systems were used and a description of these will precede the presentation of the results.

3.2 Apparatus

3.2.1 Silicon diode as a dosimeter

Silicon diodes have been employed extensively in dosimetry applications for over a decade [Jones (24)]. Our work was performed using a commercial device (Solitron CER #71). Both short circuit current and open circuit voltage modes of operation were initially investigated.

For these preliminary experiments, the diode and a Baldwin-Farmer 0.6 cm^3 ion chamber were placed side by side in a ^{60}Co beam. The diode was positioned in a closed end aluminium tube which served both as buildup layer and electromagnetic shield. No polarization voltage was applied to the PN junction and the leakage current was found to be negligible. The ion chamber was again polarized with a 300 volts battery. A variation of dose rate was achieved by raising and lowering the source from a specific point of known dose rate. A Keithley electrometer (Model 610C) was used to measure the voltage and current from the diode and the current from the ionization chamber. A digital voltmeter again monitored the electrometer output. Environmental conditions were not recorded but variations of 0.5 °C were typical and should not have affected the diode

results.

The short circuit results of the diode are presented in figure 10. As expected, the current variation is linear with dose rate. Figure 11 presents the voltage measurements obtained with an input impedance of about 10^{10} ohms. This input impedance, as figure 12 indicates, is sufficiently large to guarantee that the junction was operating in the open circuit mode. Jones (24) showed that open circuit measurements should be proportional to the logarithm of the dose rate. However, this is only approximately true for our device as figure 11 demonstrates.

The linearity with dose rate shown previously makes the short circuit mode of operation the logical choice. Moreover the time constant and the temperature dependence of the detector [Parker and Morley (25)] are also minimized by this choice.

For the results to be presented in Section 3.3, the diode was moved at constant velocity along the detector plane of figure 1. A recording of the diode current as a function of time was obtained by replacing the voltmeter by a strip-chart recorder. During each cycle, the diode crossed the field twice, thus producing two complete transmission scans. The time required for one cycle was about 0.7 minutes. By triggering the recorder's event marker at five known positions, it was possible to relate these points on the trace to the object. Some typical results will be presented.

3.2.2 X-ray film as a dosimeter

The use of film for dosimetric measurements is well recognized and is widespread in spite of the associated difficulties [Ehrlich (26)]. Moreover, the advent of automatic processors has reduced the amount of
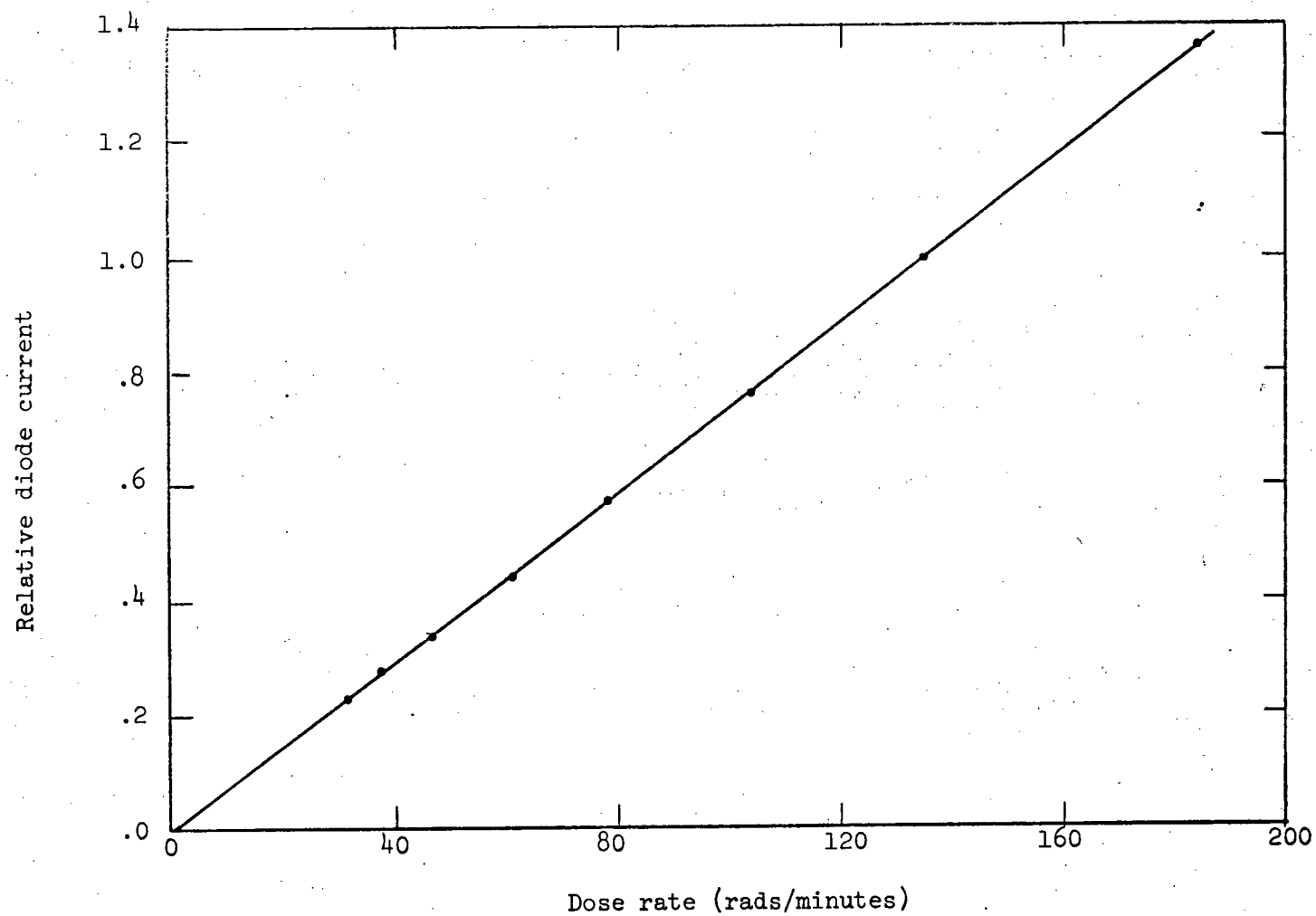
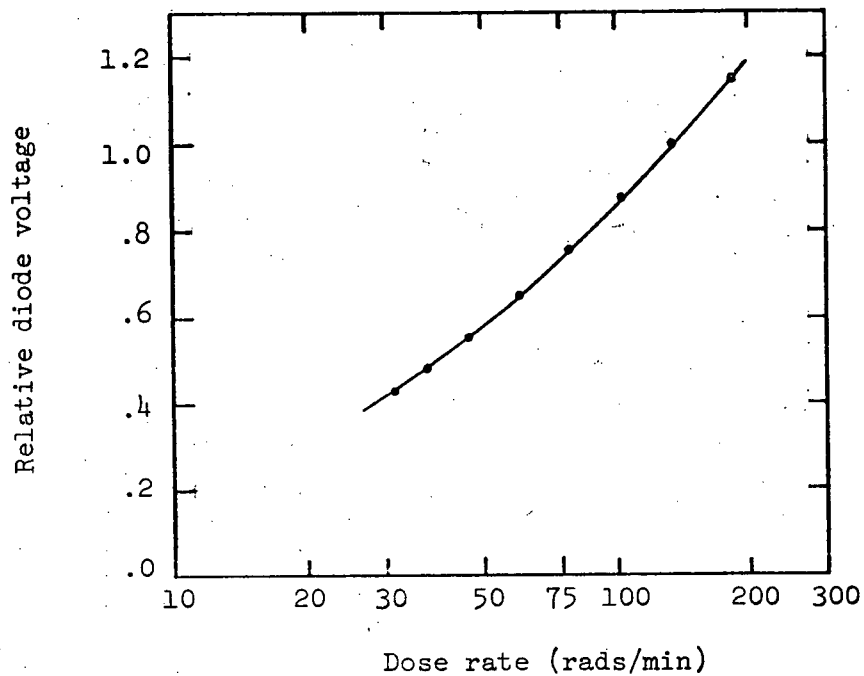FIGURE 10 SHORT CIRCUIT CHARACTERISTICS OF CER #71 DIODE

FIGURE 11   OPEN CIRCUIT VOLTAGE CHARACTERISTICS OF
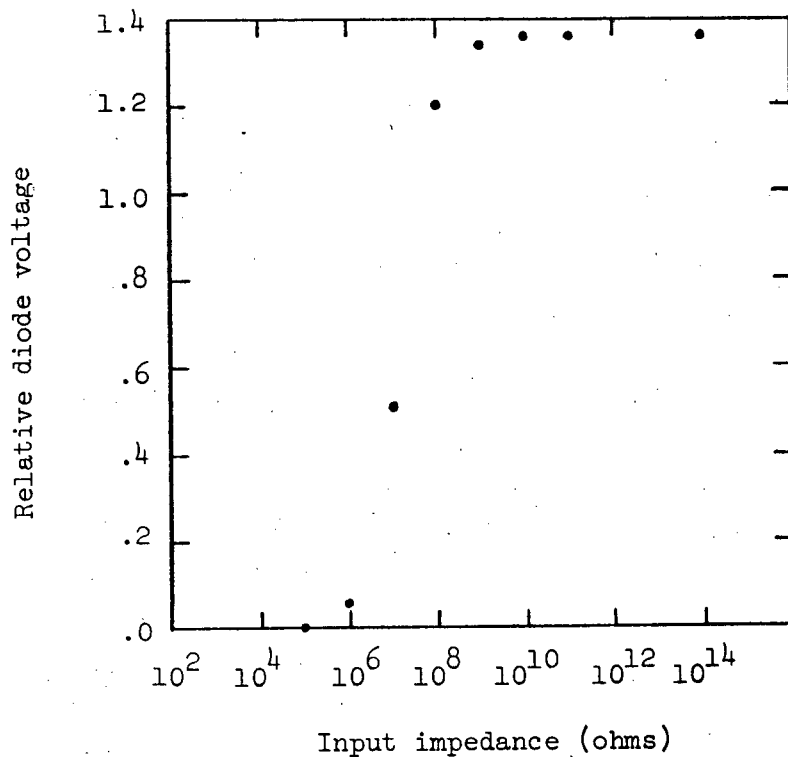CER #71 DIODE

FIGURE 12   EFFECT OF THE INPUT IMPEDANCE OF THE

MEASURING VOLTMETER ON THE DIODE RESPONSE PRODUCED

work necessary to obtain acceptable results. We have used Kodak type RP/TL (in "ready pack" form) in all our film measurements. This film is routinely used for therapy verification applications and is processible in standard medical processors.

A scanning densitometer (Kipp & Zonen, Model DD 691-D) was used for the optical density measurements. The output was displayed by a strip-chart recorder. An approximately rectangular slit of 0.01 by 0.4 cm was employed to illuminate the sample. Densities were determined with base and fog contributions included. It has been recommended by Ehrlich (26) that diffuse density determinations be made. However, the geometry of our instrument does not permit a measurement of all the optical photons scattered by the sample. Consequently, the optical densities reported in this paper are larger than the corresponding diffuse densities. A calibration strip provided with a diffuse densitometer (Macbeth Corporation, Model TD-100A) was measured with our densitometer and the results are presented in table XIII. The ratio calculated is known in sensitometry as Callier's coefficient and the trend observed here is typical [Label and Dubois (27)]. The influence of this effect must be considered when comparisons to published results are attempted.

When selected points of a specific sheet of film were irradiated by the same dose, the density uniformity achieved was ± 0.7% on the average. It was found advantageous to calibrate each film in order to eliminate the effects of variations in processing. The following procedure was used. About half of the sheet's surface was used for the measurement of interest. Then, over the remaining area, a number of points were irradiated by a ^{137}Cs unit (Picker X-ray Corporation, Model Cs-600) for different exposure times. These were measured from the unit's timer, correcting for any timer error present and are thus proportional to the dose.

TABLE XIII

COMPARISON OF MEASURED OPTICAL DENSITIES TO THE
CORRESPONDING DIFFUSE DENSITY VALUES

Diffuse density* (1)	Measured density (2)	Ratio (2)÷(1)
.20	.284	1.29
.38	.532	1.33
.58	.804	1.34
.78	1.05	1.31
.98	1.28	1.29
1.17	1.48	1.24
1.37	1.67	1.20
1.57	1.81	1.14

* From calibration strip included with diffuse densitometer indicated in text.

A source-to-film distance of about 40 cm was used and 0.5 cm of water-equivalent material provided a buildup layer. Figure 13 shows a calibration curve obtained by averaging the results of 13 films (from the same production batch) processed over a period of 45 days. Note that both scales are linear. The data from one of these films is presented in table XIV. A least-squares fit of the measured points to a third-order polynomial [Price (28)] was performed and the results of this fit are also presented in table XIV.

3.3 Inhomogeneous Phantom Measurements

These measurements were performed with a horizontal ^{60}Co beam (Eldorado 8). A rectangular field measuring 6 x 45 cm at 120 cm from
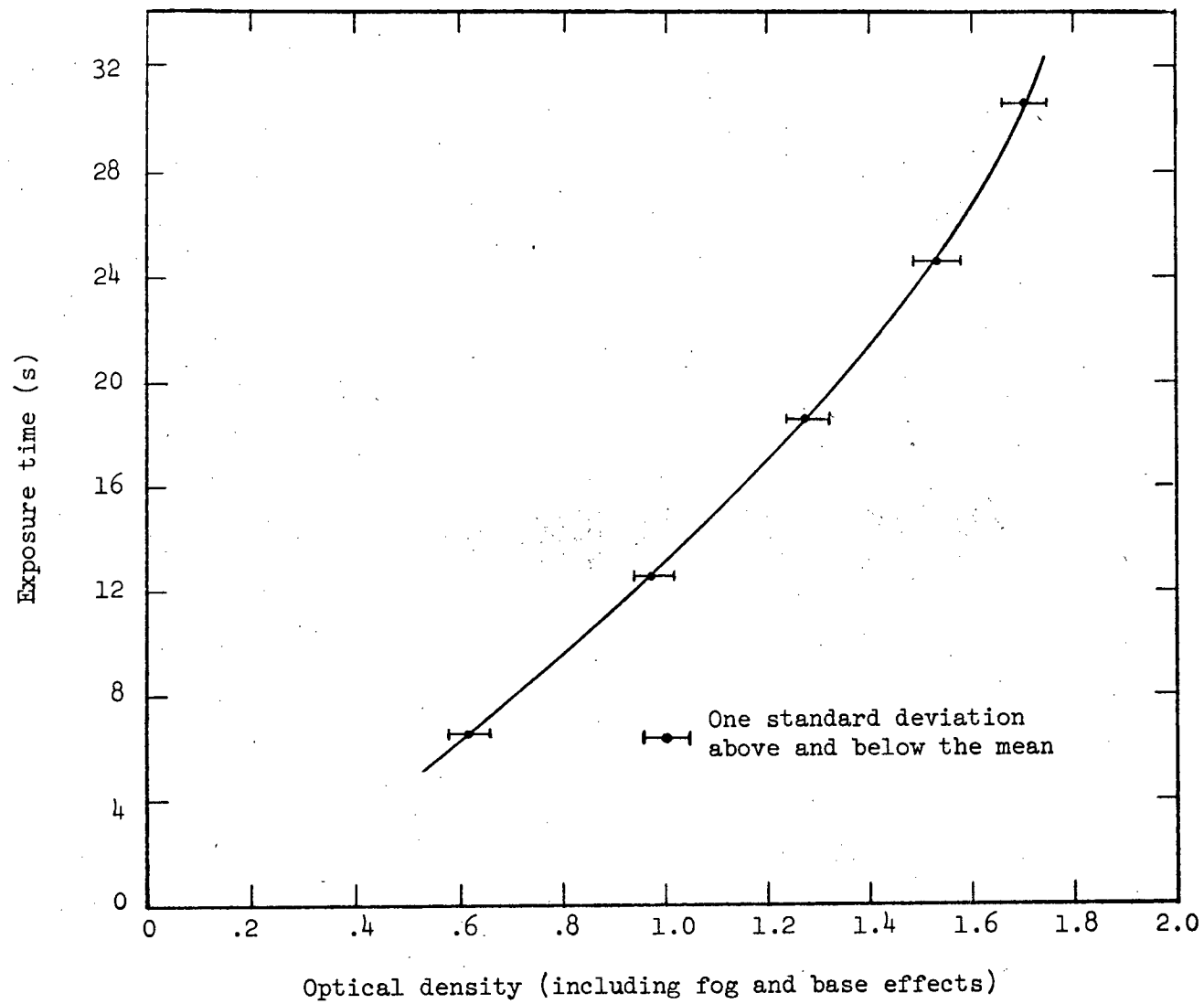
FIGURE 13 AVERAGE CALIBRATION CURVE OF RP/TL X-RAY FILM IRRADIATED

IN A ^{137}Cs BEAM

TABLE XIV

CURVE FITTING OF DENSITY VS DOSE RELATIONSHIP USING
A THIRD-ORDER POLYNOMIAL FOR KODAK RP/TL FILM

Optical density D	Irradiation time (s)	Calculated time f(D)* (s)
.578	6.61	6.58
.962	12.61	12.75
1.29_4	18.61	18.33
1.57_2	24.61	24.89
1.74_6	30.61	30.50

* $f(D) = -9.3452 + 40.083D - 27.496D^2 + 10.085D^3$ as determined by a least-squares polynomial fit.

the source was employed throughout; the absorber-to-detector distance B was 30 cm. Figure 14 shows a top view of the inhomogeneous phantom that was built. Its walls are vertical and are made of 3/16 inch perspex. They extend 10 cm above a bottom plate of the same material. Inside are positioned a 1.90 cm diameter aluminium tube and a hollow polystyrene tube of 2.53 cm inside diameter and 0.18 cm wall. The dimensions of the wood block can be determined from the figure. Lincolnshire bolus (29), a tissue-equivalent material, was used to fill the remaining volume of the phantom.

Diode scans were taken with and without the phantom in place. From these scans, the relative transmitted doses were determined at points across the field. The unattenuated beam profile was also used as a base line for the film measurements. The same geometry was used to obtain the attenuated beam profile with film. The time required to expose the film was about 0.3 minutes.

To source

Outside wall

Wood
block

Polystyrene
tube

Aluminium
cylinder

Position 22 20 18 16 14 12 10 8 6 4 2 1 3 5 7 9 11 13 15 17 19 21 23
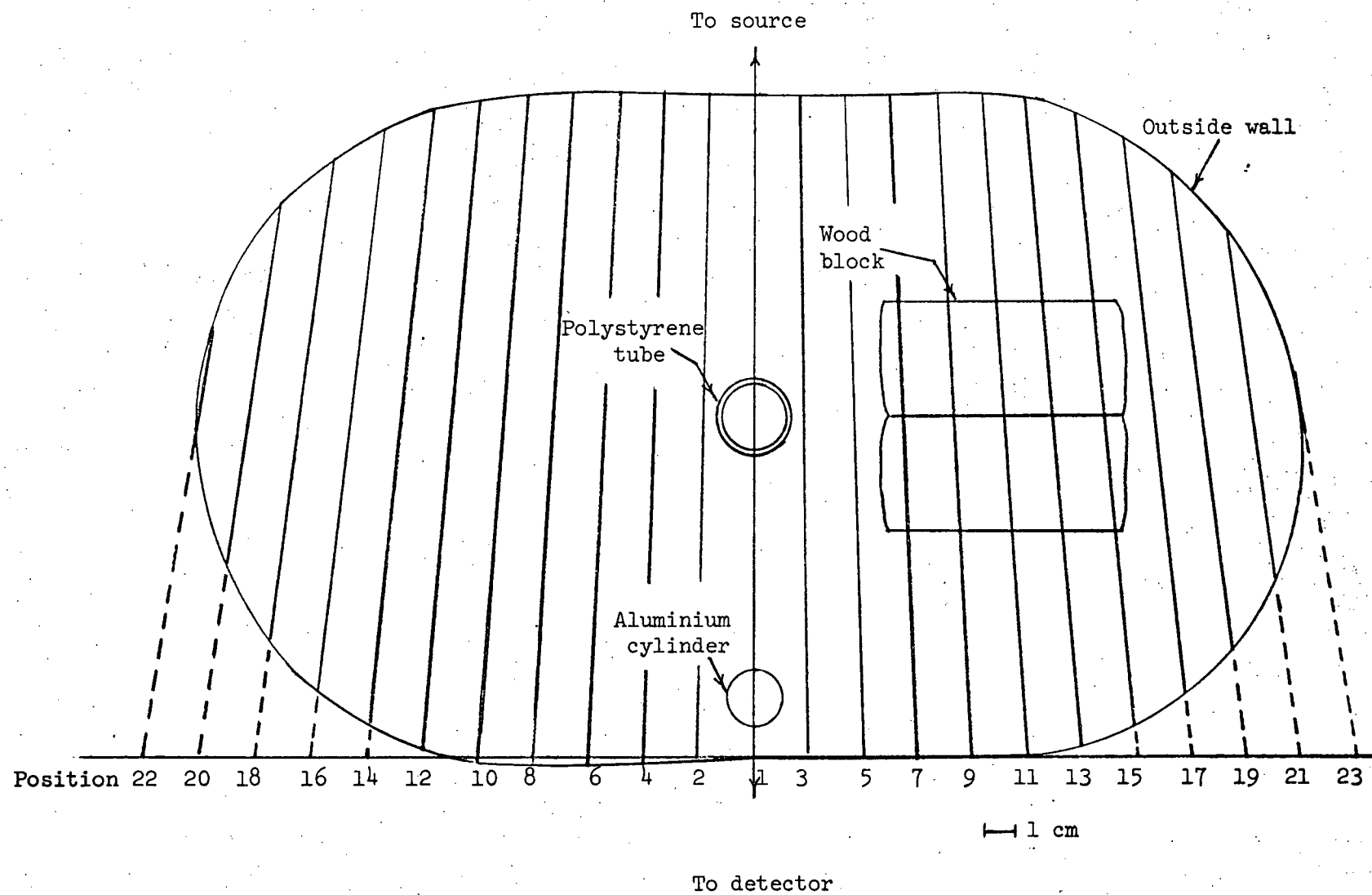
├──┤ 1 cm

To detector

FIGURE 14 TOP VIEW OF INHOMOGENEOUS PHANTOM

The results obtained from the diode and film observations are presented in table XV using the calculation method outlined in appendix C. Also shown are the equivalent thicknesses determined from the geometry of figure 14 and from the electron densities relative to water of table XVI.

The RMS difference between the equivalent thicknesses obtained from transmission data and from calculations based on the phantom's geometry and composition was estimated using the expression

$$RMS = \left[\frac{1}{n} \sum_{i=1}^{n} (t_i - \tau_i)^2 \right]^{1/2} \qquad (9)$$

where t_i = equivalent thickness along path i, determined from transmission measurements

τ_i = equivalent thickness along path i, computed from the geometry and composition of the phantom.

The obtained RMS for the average of both diode scans was 0.29 cm while it was 0.43 cm for the film observations. This is within the limit of ± 0.5 cm set at the beginning of this paper

Most workers who have performed equivalent thickness determinations have neglected to mention the accuracy attainable by their methods. Woodley et al. (17) compared the equivalent thicknesses measured using their exit dosimeter to those obtained from narrow-beam measurements. The RMS difference that they obtained at a variety of sites in humans was slightly less than 1 cm. We feel our method advantageously compares with this while offering the added capability of measuring a large number of paths simultaneously.

TABLE XV

EQUIVALENT THICKNESSES DERIVED FROM THE TRANSMISSION MEASUREMENTS
AND THE PHANTOM'S COMPOSITION AND GEOMETRY

Position	Equivalent thicknesses			
	Diode scan* #1 (cm)	Diode scan* #2 (cm)	Film* (cm)	Phantom** (cm)
1	21.35	21.35	21.34	20.75
2	20.26	20.79	20.73	20.29
4	20.22	20.42	21.00	20.34
6	20.37	20.64	20.82	20.39
8	20.84	20.81	20.61	20.45
10	20.18	20.38	20.48	20.35
12	19.95	19.62	19.78	19.90
14	18.72	18.36	18.52	18.87
16	17.14	16.83	16.67	17.13
18	15.02	14.76	14.18	14.80
20	11.88	11.06	10.86	11.17
3	20.60	20.60	20.88	20.20
5	20.30	20.47	20.91	20.22
7	17.64	18.69	18.01	17.80
9	17.23	17.26	17.52	16.83
11	16.67	16.69	16.77	16.78
13	16.32	16.47	16.68	16.40
15	15.78	15.72	16.13	15.95
17	16.53	16.46	17.00	17.07
19	14.09	15.02	14.54	14.75
21	10.46	11.75	10.62	11.00

* From transmission measurements performed with the specified detector.
** From the phantom dimensions and the electron densities of table XVI.

TABLE XVI

ELECTRON DENSITIES OF THE MATERIALS

COMPOSING THE INHOMOGENEOUS PHANTOM

Material	Electron density relative to that of water
Aluminium	2.35*
Perspex	1.15*
Polystyrene	1.03*
Water	1.000
Bolus (29)	$.957_2$**
Wood	$.490_5$**

* From the mass attenuation coefficients for 1.0 MeV photons of Hubbell (4) and density values quoted by Trent et al. (30).
** From γ-ray transmission measurements using ^{60}Co photons.

4. DISCUSSION

The measurements presented in this paper were performed with three detection systems. A Baldwin-Farmer 0.6 cm^3 ion chamber, because of its approximate energy independence was used to acquire the basic information necessary to quantify the produced scatter. The chamber does not, however, possess the spatial resolution and response speed that are required during clinical measurements.

Silicon diodes were initially investigated as possible alternatives. For silicon, the active volume per unit of ionization current produced is approximately 3,000 times smaller than that of an ion chamber. Consequently, the size needed for a particular signal level is small, resulting in an increased spatial resolution. Moreover, when operated in the short circuit current mode, they possess a faster response time than ionization chambers. Prolonged radiation exposure will produce a decrease in sensitivity of these devices and, for this reason, we have used them primarily to perform relative measurements.

From the point of view of resolution and response speed, however, film is a superior alternative. Its greater energy dependence does constitute a major drawback and one would expect this detector to be of limited value in situations where scatter is present.

In spite of this, however, film has proven to be an adequate dosimeter as the results of table XV clearly indicate. The reasons for this are illustrated in figure 4 where it is shown that the major scatter component reaching the film is due to photons scattered only once and scattered predominantly in the forward direction with minimum energy degradation.

Film, because of its ease of handling, is surely the detector of choice if routine measurements involving patients are to be performed.

We initially required that our method permit us to measure the equivalent thicknesses of an inhomogeneous phantom with a maximum inaccuracy of ± 0.5 cm. The RMS deviations that we have experimentally observed are smaller than this but we wished to confirm these estimates of the accuracy by an independent evaluation.

Figure 15 shows transmission profiles measured using the inhomogeneous phantom (figure 14). The only difference between case (a) and case (b) is that in the latter a small aluminium cylinder of 0.31 cm diameter is present in the mid-plane of the phantom. This additional 0.42 cm of water-equivalent material modifies visibly the transmission pattern as the scan indicates. Similar modifications were observed when the cylinder was moved to other positions in the phantom. The ability to detect such an object is in agreement with the previous estimate of accuracy.

We have performed no measurements of patients at this time and a complete appraisal of the method cannot be attempted before these measurements are made. We feel, however, that the method offers decided advantages over similar procedures as described in the literature, with comparable or better accuracy.
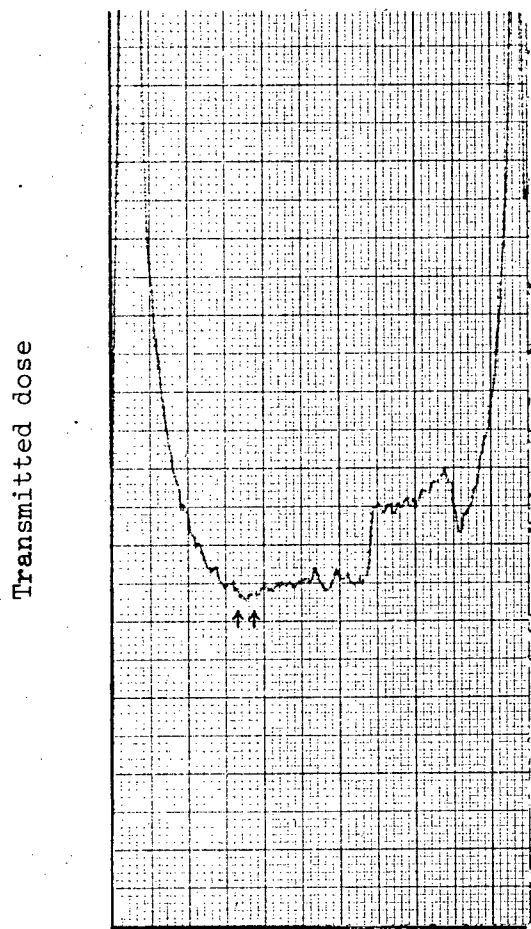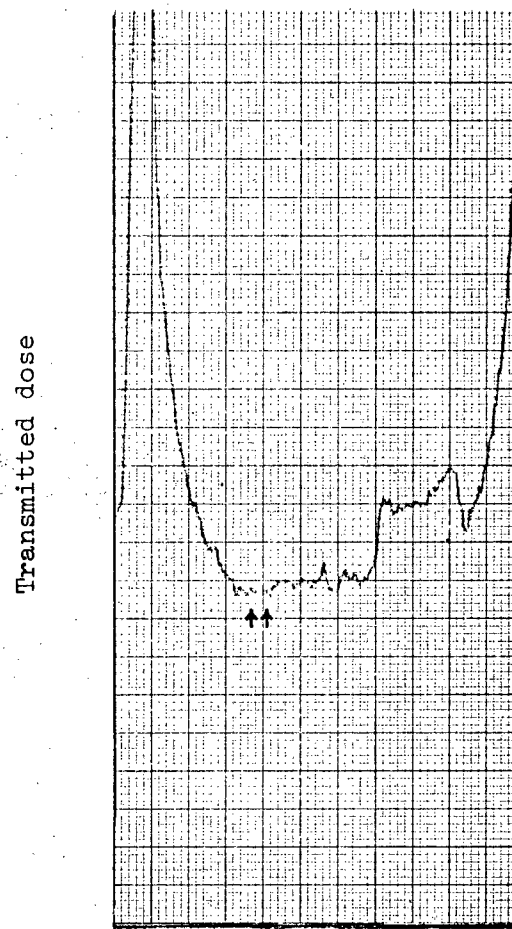
FIGURE 15   TRANSMISSION PROFILES a) WITH AND b) WITHOUT THE ADDITION OF A SMALL
ALUMINIUM ABSORBER

5. CONCLUSION

A method has been devised for the determination of water-equi-
valent thicknesses along the full width of a human transverse cross sec-
tion. Both film and commercial silicon diodes were employed to perform
the γ-ray transmission measurements. The scatter reaching the detector
was then determined using a Clarkson-type mathematical procedure and used
to calculate narrow-beam transmission data. Water-equivalent thicknesses
were then deduced using a measured linear attenuation coefficient, μ_0,
of .0653 ± .0002 cm^{-1} which is in agreement with published values. With
either detector it was possible to deduce, from transmission measurement,
the equivalent thickness along a path in an inhomogeneous phantom to better
than ± 0.5 cm. The exposure time needed to obtain the information, 0.3
and 0.7 minutes for film and diode respectively, is clinically acceptable
from the point of view of patient movement. The simpler procedure with
film makes it the choice for routine measurements involving patients.

When used with a transaxial tomography unit or any instrument
capable of producing an image of a transverse cross section, the method
will permit the determination of the electron density (relative to water)
of the various tissues present. It will then be possible to account for
the presence of these tissues when dosimetry calculations are performed
during treatment planning with beams of X rays, γ rays or heavy charged
particles.

BIBLIOGRAPHY

1. G. MARINELLO, C. MELLE, J. VILCOQ, ET AL., "Intérêt de la tomographie axiale en position couchée pour la préparation des malades à la radiothérapie". Journal de Radiologie, de l'Electrologie et de Médecine Nucléaire, 54, 841-847, 1973.

2. P.V. HOUDEK, K.K. CHARYULU, A. SUDARSANAM, ET AL., "Role of transverse axial tomography in three dimensional treatment planning". Radiology, 112, 409-412, 1974.

3. S. TAKAHASHI, "An atlas of axial transverse tomography and its clinical application" (Springer-Verlag, New York, 1969).

4. J.H. HUBBELL, "Photon cross sections, attenuation coefficients, and energy absorption coefficients from 10 KeV to 100 GeV", NSRDS-NBS 29 (U.S. Government Printing Office, Washington, 1969).

5. Y.S. KIM, "Human tissues: Chemical compositions and photon dosimetry data". Radiation Research, 57, 38-45, 1974.

6. H.Q. WOODARD, "The elementary composition of human cortical bone". Health Physics, 8, 513-517, 1962.

7. INTERNATIONAL COMMISSION ON RADIATION UNITS AND MEASUREMENTS, "ICRU Report 10b: Physical aspects of irradiation", National Bureau of Standards Handbook 85 (U.S. Government Printing Office, Washington, 1964), p. 4.

8. P. DALTON, J.E. TURNER, "New evaluation of mean excitation energies for use in radiation dosimetry". Health Physics, 15, 257-262, 1968.

9. T.H. ALLEN, H.J. KRZYWICKI, J.E. ROBERTS, "Density, fat and solids in freshly isolated tissues". Journal of Applied Physiology, 14, 1005-1008, 1959.

10. J.M. DEBOIS, M. de ROO, "Experimental demonstration of the influence of bone on dose distribution in radiotherapy". Radiology, 92, 1-10, 1969.

11. INTERNATIONAL COMMISSION ON RADIATION UNITS AND MEASUREMENTS, "ICRU Report 10d: Clinical dosimetry", National Bureau of Standards Handbook 87 (U.S. Government Printing Office, Washington, 1963), p. 24.

12. F.W. SPIERS, "Effective atomic number and energy absorption in tissues". British Journal of Radiology, 19, 52-63, 1946.

13. R. GOLDEN, J.H. CUNDIFF, W.H. GRANT III, ET AL., "A review of the activities of the AAPM Radiological Physics Center in interinstitutional trials involving radiation therapy". Cancer, 29, 1468-1472, 1972.

14. J.G. HOLT, J.S. LAUGHLIN, "A practical method of obtaining density distribution within patients". Radiology, 93, 161-166, 1969.

15. P.M. PFALZNER, "Rotation therapy with a cobalt 60 unit, II Transit dose measurements as a means of correcting tumour dose for non-waterequivalent absorbing media". Acta Radiologica, 45, 62-68, 1956.

16. S.O. FEDORUK, H.E. JOHNS, "Transmission dose measurement for cobalt-60 radiation with special reference to rotation therapy". British Journal of Radiology, 30, 190-195, 1957.

17. R.G. WOODLEY, E.L. BRONSTEIN, J.S. LAUGHLIN, "Exit dosimeter for effective patient thickness". Radiology, 74, 273-278, 1960.

18. INTERNATIONAL COMMISSION ON RADIATION UNITS AND MEASUREMENTS, "ICRU Report 18: Specification of high activity gamma-ray sources" (International Commission on Radiation Units and Measurements, Washington, 1970), p. 13.

19. E. STORM, H.I. ISRAEL, "Photon cross sections from 1 KeV to 100 MeV for elements Z=1 to Z=100". Nuclear Data Tables, A7, 565-681, 1970.

20. D.E.A. JONES, C. GREGORY, I. BIRCHALL, "Dosage distribution in rotational cobalt-60 therapy". British Journal of Radiology, 29, 196-201, 1956.

21. H.E. JOHNS, E.R. EPP, D.V. CORMACK, S.O. FEDORUK, "Depth dose data and diaphragm design for the Saskatchewan 1000 curie cobalt unit". British Journal of Radiology, 25, 302-308, 1952.

22. W.H. PAYNE, R.G. WAGGENER, L.B. LEVY, ET AL., "A comparison of central-axis depth-dose values in water and tissue-equivalent liquids for ^{60}Co". Medical Physics, 1, 277-279, 1974.

23. J.R. CLARKSON, "A note on depth doses of fields of irregular shape". British Journal of Radiology, 14, 265-268, 1941.

24. A.R. JONES, "The application of some direct current properties of silicon junction detectors to γ-ray dosimetry". Physics in Medecine and Biology, 8, 451-459, 1963.

25. R.P. PARKER, B.J. MORLEY, "Silicon PN junction surface barrier detectors and their application to the dosimetry of X and gamma-ray beams". In "Symposium on solid state and chemical radiation dosimetry in medecine and biology" (International Atomic Energy Agency, Vienna, 1967), p. 167.

26. M. EHRLICH, "Photographic dosimetry of X and γ-rays". National Bureau of Standards Handbook 54 (U.S. Government Printing Office, Washington, 1954).

27. L. LOBEL, W. DUBOIS, "Basic sensitometry", second edition (Focal Press, London, 1967), p.53.

28. C. PRICE, "A method of determining the sensitometric properties of non-screen X-ray films". British Journal of Radiology, 46, 719-723, 1973.

29. D.D. LINDSAY, B.E. STERN, "A new tissue-like material for use as bolus". Radiology, 60, 355-362, 1953.

30. H.M. TRENT, D.E. STONE, R.B. LINDSAY, "Density of solids". In "American Institute of Physics Handbook", D.E. Gray, coordinating editor (McGraw-Hill, Toronto, 1957), pp. 2-17, 2-34.

31. C.M. DAVISSON, R.B. EVANS, "Gamma-ray absorption coefficients". Reviews of Modern Physics, 24, 79-107, 1952.

32. R.D. EVANS, "X-ray and γ-ray interaction". In "Radiation Dosimetry, volume 1", second edition, F.H. Attix and W.C. Roesch, editors (Academis Press, New York, 1968), table XXIII, p. 136.

33. C.G.A. AIRD, F.T. FARMER, "The design of a thimble chamber for the Farmer dosimeter". Physics in Medecine and Biology, 17, 169-174, 1972.

34. G.P. BARNARD, E.J. AXTON, A.R.S. MARSH, "A study of cavity ion chambers for use with 2 MV X-rays: Equilibrium wall thickness: Wall absorption correction". Physics in Medecine and Biology, 3, 366-394, 1959.

35. W.R. BRUCE, H.E. JOHNS, "The spectra of X rays scattered in low atomic number materials", British Journal of Radiology Supplement #9 (British Institute of Radiology, London, 1960), pp. 6-7.

APPENDIX A

CALCULATION OF FIRST SCATTER FOR THE GENERAL CASE

Figure A1 illustrates the conditions under which the calculation is performed. We assume a monoenergetic source of 1.25 MeV photons falling on an annular ring of volume $2\pi y dy dx$. We wish to evaluate the number of photons dN_1 scattered only once at an angle θ from this annular ring and reaching the detector. From Davisson and Evans (31),

$$dN_1 = [N_0(\cos^2\phi_0/(A-x)^2)2\pi y dy \exp(-\mu_0(x_0-x)\sec\phi_0)] \ [K(\theta)\rho_e dx]$$
$$[\exp(-\mu_1 x\sec\phi_1)] \ [s(\sec\phi_1)\epsilon(\theta)/((B+x)^2\sec^2\phi_1)] \qquad (A-1)$$

where N_0 = number of photons emitted by the source per unit time.

   s = area of plane detector.

$K(\theta)$ = Compton cross section of the number of photons scattered per unit solid angle in the direction θ. (cm^2/electron)

$K(\theta) = r_0^2[1+\alpha(1-\cos\theta))^{-2} \ (1+\cos^2\theta+(\alpha^2 \ (1-\cos\theta)^2)/(1+\alpha(1-\cos\theta)))]/2$.

$K(\theta) = r_0^2 k(\theta)/2$.

$\epsilon(\theta)$ = energy dependence of detector relative to 1.25 MeV photons.

   r_0 = classical radius of the electron

   $r_0 = 2.818 \cdot 10^{-13}$ cm.

   ρ_e = electron density of the scatterer.

   $\rho_e = 3.344 \cdot 10^{23}$ electrons/cm^3 for water.

   μ_0 = narrow-beam attenuation coefficient of the primary 1.25 MeV photons.

   $\mu_0 = .0653 \ cm^2$/g for water.

   μ_1 = attenuation coefficient of the scattered photons neglecting photoelectric absorption.

   $\mu_1 = \mu_0 f(\alpha')/f(\alpha)$.

$f(\alpha) = 2\pi r_0^2 \ ((1+\alpha)/\alpha^2) \ ((2(1+\alpha)/(1+2\alpha)) - \alpha^{-1}\ln(1+2\alpha)) + (2\alpha)^{-1}\ln(1+2\alpha) - (1+3\alpha)/(1+2\alpha)^2)$.

α = energy of primary photons in units of electron mass.

α = 1.25/.5110.

α' = energy of scattered photons in units of electron mass.

α' = $\alpha/(1+\alpha(1-\cos\theta))$.

The description of the equation is reproduced from Davisson and Evans:

> "The first bracket in the equation is the number of photons incident on the annular ring per second; the second bracket is the fraction of the photons scattered per unit solid angle in the direction θ; the third represents the loss in the number of scattered photons due to absorption in the absorber; and the last bracket is essentially the solid angle subtended by the detector at any point of the scattering volume."

The number of primary photons measured by the detector without the absorber is $N_0 s/(A+B)^2$. Then, from equation (A-1), the relative number of photons singly scattered dF_1 from the volume element is

$$dF_1 = .08343[(A+B)/((A-x)(B+x))]^2 \cos^2\phi_0 \cos\phi_1$$
$$\exp[-\mu_0(x_0-x)\sec\phi_0 - \mu_1 x \sec\phi_1] k(\theta)\varepsilon(\theta)dxdy \qquad \text{(A-2)}$$

where $.08343 = \pi r_0^2 \rho_e$.

The measured ionization current is assumed proportional to the energy, $d\Delta_1$, absorbed in the perspex cap of the chamber. For dF_1 photons

$$d\Delta_1 = dF_1 \alpha' \mu_{en}(\alpha')/\mu_{en}(\alpha) \qquad \text{(A-3)}$$

where $\mu_{en}(\alpha)/\rho$ = mass energy absorption coefficient of perspex at energy α.

By integrating equation (A-3), it is possible to determine the first scatter reaching P,

$$\Delta_1 = \int_0^R \int_0^{x_0} d\Delta_1 \qquad \text{(A-4)}$$

where x_0 = total absorber thickness.

R = field radius of circular field measured at depth (x_0-x). It is, for a diverging beam, a function of the thickness x.
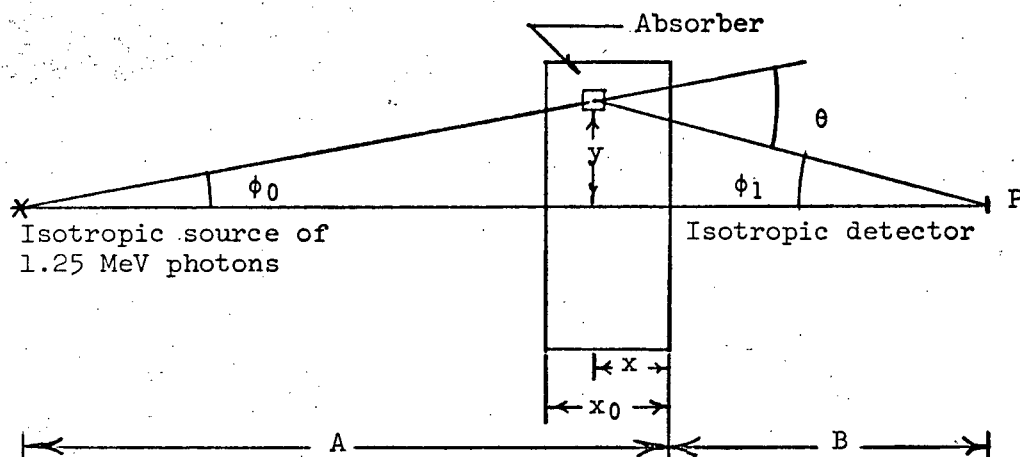
FIGURE A1 DIAGRAM ILLUSTRATING THE CALCULATION OF THE FIRST SCATTER
REACHING A POINT P POSITIONED AT A DISTANCE B FROM THE SCATTERER
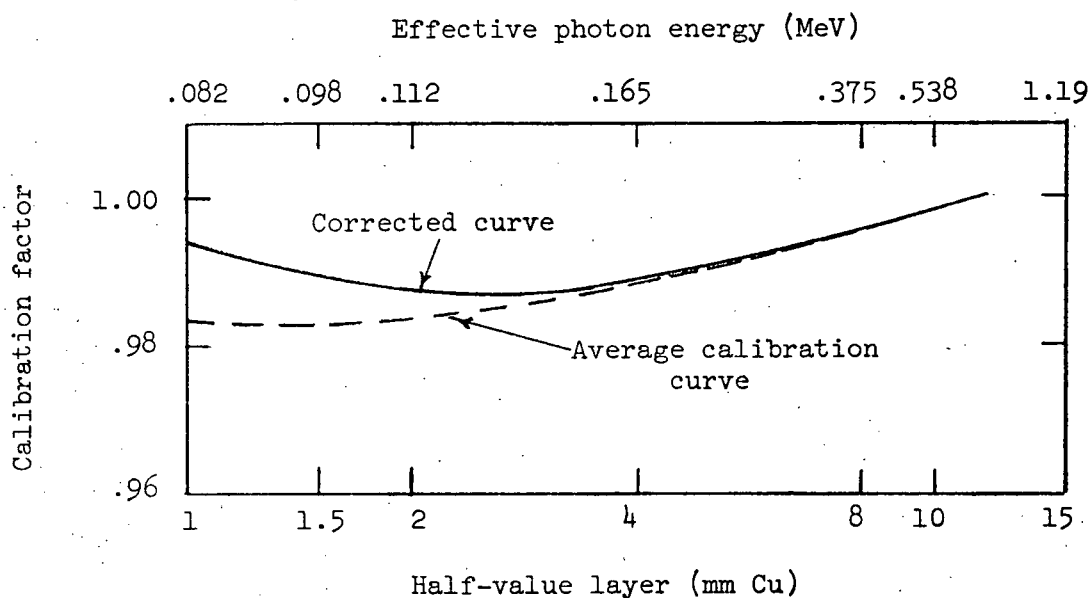[Adapted from Davisson and Evans (31)]

FIGURE A2 CALIBRATION CURVE FOR THE BALDWIN-FARMER 0.6 cm^3
CHAMBER CORRECTED FOR THE PRESENCE OF THE BUILDUP CAP

$$R = R_0(A-x)/A.$$

R_0 = field radius of circular field at distance A from the source.

Equation (A-4) was evaluated by numerical integration. The following relations were used to express equation (A-3) in terms of the variables x and y only,

$$\phi_0 = \text{Arc tan}(y/(A-x))$$

$$\phi_1 = \text{Arc tan}(y/(B+x))$$

$$\theta = \phi_0 + \phi_1. \qquad\qquad (A-5)$$

Evans (32) has tabulated values of μ_{en}/ρ for perspex. His data can be fitted, for photon energies between 0.10 and 1.25 MeV, by the empirical expression,

$$\mu_{en}(\alpha)/\rho = (.0352-.0026\alpha)/(1+.455 \exp(-4.29(\alpha-.196))). \quad (A-6)$$

Table AI shows the quality of the fit.

The energy dependence, $\varepsilon(\theta)$, of the Baldwin-Farmer 0.6 cm^3 ion chamber used in our experiments is not known. Our chamber is of an older design for which typical calibration curves have been recently published (33). An average of these calibration curves is presented in figure A2. The calibration was made relative to 2 MV X rays at the National Physical Laboratory.

A difference between calibration and experimental conditions does exist, however. During our measurements, the ion chamber was permanently fitted with a buildup cap suitable for irradiation in a ^{60}Co beam. The presence of this additional absorbing material must be accounted for and suitable corrections applied to the calibration curve before $\varepsilon(\theta)$ can be inferred from it. Figure A2 shows the effect of this correction using some results of Barnard et al. (34). The energy variation is then of the order of 0.7% over the range of half-value layers extending from

TABLE AI

COMPARISON OF EVANS' TABULATED VALUES OF μ_{en}/ρ (32) FOR

PERSPEX TO THE VALUES USED IN THE CALCULATIONS

α	μ_{en}/ρ	
	Tabulated (cm^2/g)	Calculated* (cm^2/g)
.1957	.0238	.0238
.2935	.0265	.0265
.3914	.0286	.0287
.5871	.0310	.0310
.7828	.0320	.0318
.9785	.0321	.0322
1.174	.0319	.0319
1.566	.0311	.0311
1.957	.0301	.0301
2.935	.0275	.0275
* From equation (A-6).		

1 to 12 mm of copper. We thus feel justified in neglecting this effect
and $\varepsilon(\theta) = 1$ was used throughout the calculations.

APPENDIX B

CALCULATION OF FIRST SCATTER AT THE EXIT SURFACE OF AN ABSORBER

Bruce and Johns (35) have described a method to calculate the first scatter contribution inside a water phantom irradiated by circular photon beams of various energies. The method can be applied to the exit dose situation by simply neglecting the backscatter contribution.

Figure B1 is adapted from their paper and defines some of the quantities used. The relative energy fluence dI_1 for photons of energy between $h\nu'$ and $h\nu' + dh\nu'$ scattered at an angle θ is

$$dI_1 = \rho_e h\nu'/h\nu (d\sigma/dh\nu')[(\exp(-\mu_0 x_0))/(\mu_1 - \mu_0 \cos\theta)]$$
$$[1 - \exp(-(\mu_1 - \mu_0 \cos\theta)x_m)]\, dh\nu' \qquad (B-1)$$

where $d\sigma/dh\nu'$ = Compton cross section of the number of photons scattered per unit energy interval at energy $h\nu'$.

$$= \pi r_0^2 (\alpha h\nu)^{-1}[(1+\cos^2\theta)+\alpha^2(1-\cos\theta)^2/(1+\alpha(1-\cos\theta))].$$

$h\nu$ = incident photon energy = 1.25 MeV

$h\nu'$ = scattered photon energy

$$= h\nu/(1+\alpha(1-\cos\theta)).$$

x_m = maximum absorber thickness between the edge of the beam and the point P.

The meaning of the other symbols is specified in appendix A.

Δ_1 can then be determined by integration with respect to the energy of the scattered photon,

$$\Delta_1 = \int_{h\nu_{min}}^{h\nu} dI_1 \mu_{en}(\alpha')/\mu_{en}(\alpha) \qquad (B-2)$$

where $h\nu_{min}$ = minimum energy of the photons scattered in the forward direction reaching P.
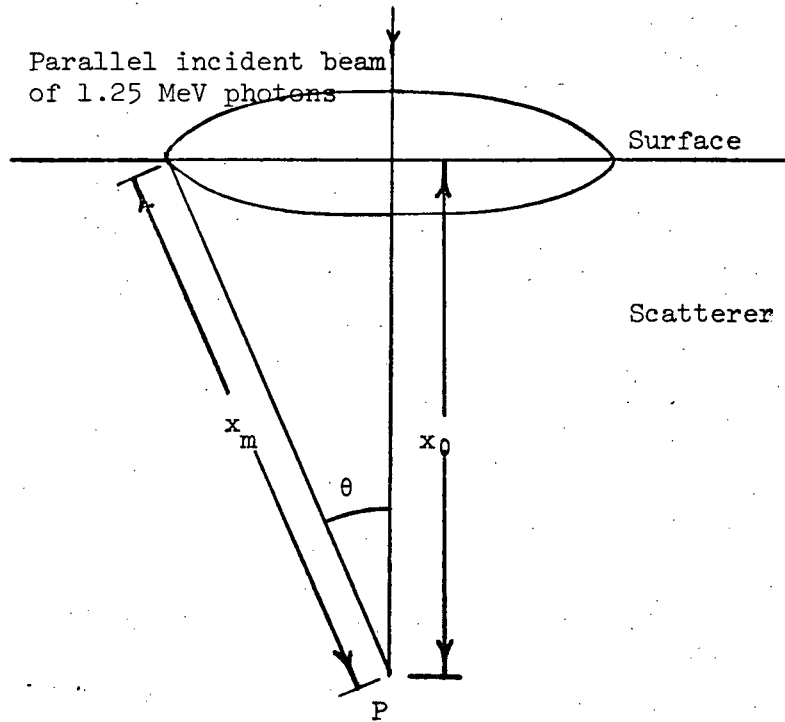
$$= h\nu/(1+\alpha).$$

FIGURE B1   DIAGRAM TO ILLUSTRATE THE CALCULATION
OF THE FIRST SCATTER REACHING A POINT P INSIDE AN
HOMOGENEOUS SCATTERER
[Adapted from Bruce and Johns (35)]

In this paper, equation (B-2) was evaluated as a summation extending from 0.35 to 1.25 MeV by 0.10 MeV intervals.

APPENDIX C

CALCULATION OF THICKNESSES FROM TRANSMISSION MEASUREMENTS

The mathematical method employed to calculate water-equivalent thicknesses from transmission results is described here.

The measurements yield values of relative transmitted dose T at points distributed along a line in the detector plane. This line corresponds to a geometrical projection of the longitudinal axis of the rectangular ^{60}Co beam. The field dimensions, at 120 cm from the source, are 6 x 2b where 2b is the length of the longitudinal side. Mathematically,

$$T = T(P_i, b, t_i) \qquad (C-1)$$

where P_i = distance of point i off the central axis of the field, (i = 1,...,n).

t_i = water-equivalent thickness along the path joining the source and point i.

Since t_i is related to the primary transmitted dose, $\exp(-\mu_0 t_i)$, we can write, from equation (3),

$$t_i = [\ln[T(P_i, b, t_i) - \Delta(P_i, b, t_i)]]/-\mu_0 \qquad (C-2)$$

The quantity $\Delta(P_i, b, t_i)$ must then be evaluated in the general case where the absorber is an inhomogeneous body. We have assumed for this evaluation that the primary beam is uniform over the length of the field.

We consider the case where the points, i, are equally distributed along the measurement line. This is shown in figure C1 for the case where n = 5. Similarly, we segment the radiation beam into n smaller beams indexed as shown.

At each point i, we then write

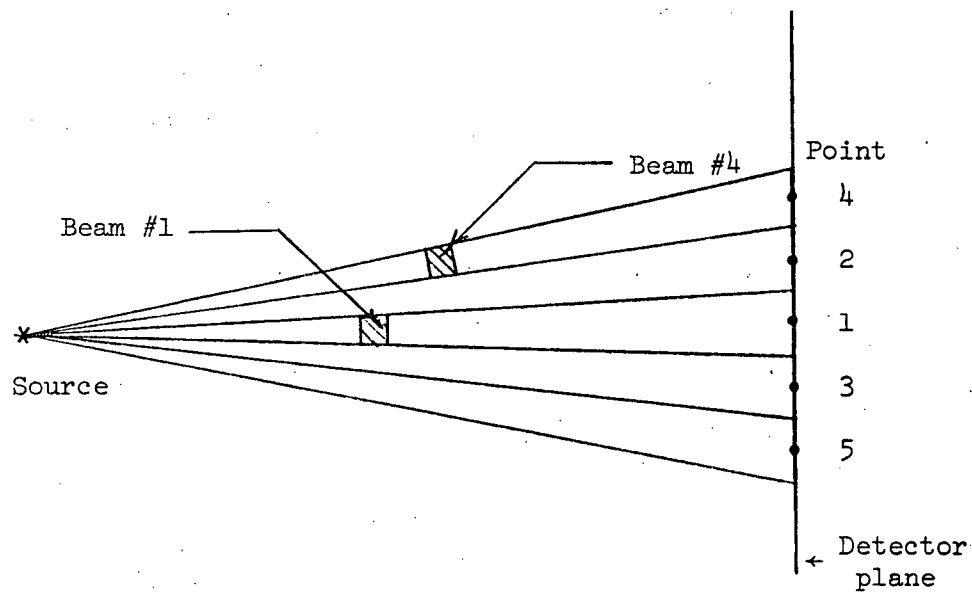$$\Delta(P_i, b, t_i) = \sum_{j=1}^{n} \Delta(P_i, b/n, t_j) \qquad (C-3)$$

FIGURE C1   ILLUSTRATION OF THE GEOMETRY USED TO CALCULATE
THE SCATTER REACHING THE MEASUREMENT POINTS

where $\Delta(P_i,b/n,t_j)$ = relative scatter reaching point i from beam j.

t_j = water-equivalent thickness along the path joining the source and the point j.

In the particular case of points on the central axis of the rectangular beam (i.e., point 1 in figure C1), the determination of the terms of equation (C-3) follows from the results presented in section 2.3. Thus,

$$\Delta_{i=j}(P_i,b/n,t_i) = \Delta(0,b/n,t_i)$$

$$\Delta_{j\ odd}(P_i,b/n,t_j) = [\Delta(0,jb/n,t_j') - \Delta(0,(j-1)b/n,t_j')]/2$$

$$\Delta_{j\ even}(P_i,b/n,t_j) = [\Delta(0,(j+1)b/n,t_j') - \Delta(0,jb/n,t_j')]/2 \quad (C-4)$$

where $t_j' = t_j\ cos\theta_j$

θ_j = Arc tan$[(j-2)b/n/120]$, j=3,5,...

= Arc tan$[(j-1)b/n/120]$, j=2,4,...

For the general case of points off the axis of the original beam, the calculation is performed in a similar fashion assuming the validity of the procedure described in the text.

The calculations performed in section 3.3 were based on an iterative procedure. We initially assumed specific thicknesses t_i and solved equations (C-2) and (C-3). The newly determined thickness values were then incorporated in equations (C-2) and (C-3) and a new solution obtained. The procedure was continued until a specific criterion of convergence was satisfied. Usually a few iterations were sufficient to ensure that the variation of $\Delta(P_i,b,t_i)$ was less than 1% and thus well within the experimental accuracy.